iScience

CellPress
OPEN ACCESS

Article

Modulation of itch and pain signals processing in ventrobasal thalamus by thalamic reticular nucleus

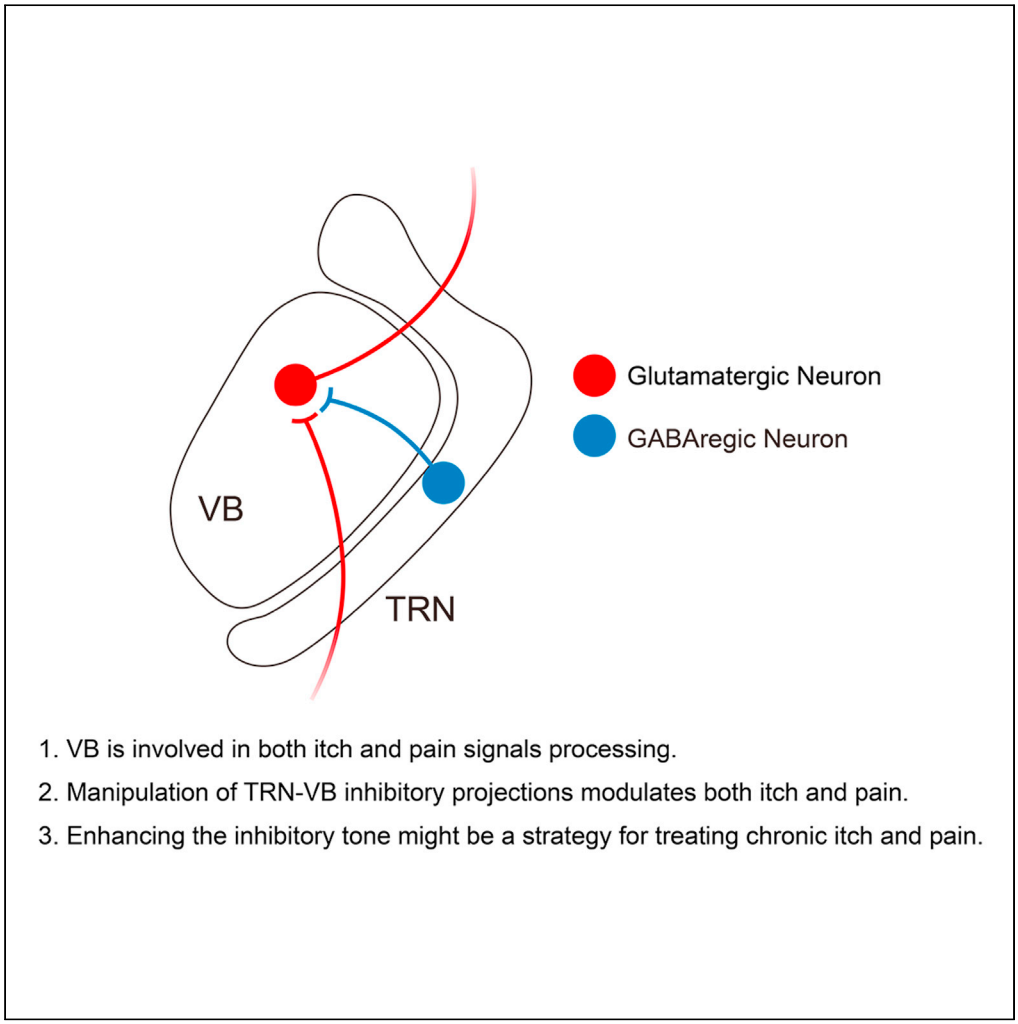

Peng-Fei Liu, Yan Wang, Ling Xu, ..., Jin-Bao Li, Ling Zhang, Di Mu

lzhang0808@tongji.edu.cn (L.Z.)
damonmu@163.com, dimu08207@ustc.edu (D.M.)

Highlights

VB is involved in both itch and pain signals processing

Manipulation of VB or TRN-VB inhibitory projections modulates both itch and pain

Enhancing the inhibitory tone might be a strategy for treating itch and pain

Liu et al., iScience 25, 103625
January 21, 2022
https://doi.org/10.1016/j.isci.2021.103625

iScience

CellPress
OPEN ACCESS

Article

Modulation of itch and pain signals processing in ventrobasal thalamus by thalamic reticular nucleus

Peng-Fei Liu,[1,4] Yan Wang,[1,4] Ling Xu,[1,4] An-Feng Xiang,[2,4] Ming-Zhe Liu,[3] Ya-Bing Zhu,[1] Xin Jia,[2] Rui Zhang,[1] Jin-Bao Li,[1] Ling Zhang,[2,*] and Di Mu[1,5,*]

SUMMARY

Thalamic reticular nucleus (TRN) is known to be crucial for dynamically modulating sensory processing. Recently, the functional role of TRN in itch and pain sensation processing has drawn much attention. We found that ventrobasal thalamus (VB) neurons exhibited scratching behavior-related and nociceptive behavior-related neuronal activity changes, and most of VB neurons responsive to pruritic stimulus were also activated by nociceptive stimulus. Inhibition of VB could relieve itch-induced scratching behaviors and pathological pain without affecting basal nociceptive thresholds, and activation of VB could facilitate scratching behaviors. Tracing and electrophysiology recording results showed that VB mainly received inhibitory inputs from ventral TRN. Furthermore, optogenetic activation of TRN-VB projections suppressed scratching behaviors, and ablation of TRN enhanced scratching behaviors. In addition, activation of TRN-VB projections relieved the pathological pain without affecting basal nociceptive thresholds. Thus, our study indicates that TRN modulates itch and pain signals processing via TRN-VB inhibitory projections.

INTRODUCTION

Itch and pain are both unpleasant sensations that serve as critical protective mechanisms. Exciting progress has been made in deciphering the mechanisms of itch and pain at both the peripheral and central nervous system levels (Chen and Sun, 2020; Dong and Dong, 2018; Huang et al., 2018; Koch et al., 2018; Kuner and Kuner, 2021; Meixiong and Dong, 2017). Recent studies have begun to dissect the functional roles of ascending projections from the spinal cord to the brain in itch and pain (Deng et al., 2020; Huang et al., 2019; Mu et al., 2017). The thalamus is the primary relay nucleus receiving ascending projections from the spinal cord and thought to process the sensation component of itch and pain (Basbaum et al., 2009; Chen and Sun, 2020; Kuner and Kuner, 2021; Todd, 2010). Brain imaging studies in humans and rats have shown that the thalamus is activated in itch and pain (Jeong et al., 2016; Mochizuki et al., 2013; Mochizuki and Kakigi, 2015; Tinnermann et al., 2021).

A series of *in vivo* electrophysiological studies have examined the spinothalamic tract neurons (Davidson et al., 2007, 2012), trigeminothalamic tract neurons (Moser and Giesler, 2014), and thalamic neurons (Lipshetz et al., 2018) in response to itch and nociceptive stimuli. Their results showed that the majority of examined neurons in the spinal cord and thalamus were excited by both pruritic and nociceptive stimuli in anesthesia state, raising the question of whether there are itch-specific or pain-specific neurons in the thalamus. The anesthesia state might affect neuronal responses to itch and pain in these studies. The relationship of itch-responsive and pain-responsive neurons in free-moving mice needs to be determined.

The ventrobasal thalamus (VB) is the primary projection target in the thalamus (Gauriau and Bernard, 2004). Chemical or electrolytic lesions or reversible inhibition of VB attenuated nociceptive behaviors (Saade et al., 2006). Most of the VB neurons are excitatory neurons, and the major inhibitory input of VB comes from the thalamic reticular nucleus (TRN) (Halassa and Acsady, 2016; Li et al., 2020; Zhang et al., 2018). The TRN modulates sensorimotor processing, cognitive function, selective attention, and nociceptive

[1]Department of Anesthesiology, Shanghai General Hospital, Shanghai Jiao Tong University School of Medicine, Shanghai 201620, China

[2]The First Rehabilitation Hospital of Shanghai, Tongji University School of Medicine, Shanghai 200090, China

[3]Department of Respiratory, The First Affiliated Hospital of Guangzhou Medical University, Guangzhou 510120, China

[4]These authors contributed equally

[5]Lead contact

*Correspondence: lzhang0808@tongji.edu.cn (L.Z.)

*Correspondence:: damonmu@163.com, dimu08207@ustc.edu (D.M.)

https://doi.org/10.1016/j.isci.2021.103625

information (Dong et al., 2019; Halassa and Acsady, 2016; Halassa et al., 2014; Marlinski et al., 2012; Zhang et al., 2017). Previous studies have shown that activation of GABA receptors in the VB or activation of TRN-VB projections induced antinociception in inflammatory pain (Potes et al., 2006; Zhang et al., 2017). However, the functional role of TRN-VB in itch processing is still elusive.

In our study, we first examined the neuronal activity of VB neurons in response to itch and pain via *in vivo* fiber photometry recording and extracellular recording. Then we manipulated the activity of VB and examined the itch-related and pain-related behaviors. Furthermore, we dissected the characteristics of TRN-VB inhibitory projections and deciphered the functional roles of TRN in modulating itch and pain.

RESULTS

Neuronal activity of the VB neurons in itch and pain

We first examined the calcium activity of the VB by performing *in vivo* fiber photometry in freely moving mice. Adeno-associated virus (AAV) expressing the calcium indicator GCaMP6s (AAV-hSyn-GCaMP6s) or AAV-hSyn-EGFP was injected into the contralateral VB (according to pruritogens injection side) of wild-type mice, and optical fibers were implanted into the VB (Figures S1A–S1E). Mouse scratching behavior was synchronously recorded using a magnetic induction method (Figure S1F) (Mu et al., 2017). We found that the GCaMP6s fluorescence signals of the VB were elevated during pruritogens-induced scratching trains (Figures S1G–S1M).

To determine the dynamics of the VB neuronal activity during itch and pain, we next performed extracellular recording in behaving mice during itch-induced scratching behavior and nociceptive mechanical stimulus (Figures 1A–1C). A total of 52 units representing neuronal activity in VB were consistently recorded and recognized in histamine, chloroquine, and nociceptive mechanical stimuli sessions. We found a significant percentage of VB neurons displayed elevated activity near the onset of the scratching trains induced by histamine (75%, 39/52 units, Figures 1D–1G). In contrast, a small percentage of VB neurons exhibited decreased activity (8%, 4/52 units). Similarly, 69% of VB neurons showed increased activity (36/52 units), whereas 8% of VB neurons showed decreased activity (4/52 units) in the chloroquine (non-histaminergic dependent pruritogen) model (Figures 1G and S2A). Besides, we found that 60% (31/52) units exhibited elevated activity patterns following histamine-induced and chloroquine-induced scratching onset (Figure 1G), which were defined as itch-scratching-activated units. These results indicate that VB neuronal activities are strongly correlated with scratching behaviors.

We further examined the neuronal activities of the VB neurons during nociceptive mechanical stimulus in the neck (2.0 g von Frey filament). 67% of the units recorded showed increased activity in response to 2.0 g von Frey nociceptive mechanical stimulus (35/52 units, Figures 1H and S2B). We further analyzed the activity patterns of itch-scratching-activated units in the nociceptive mechanical model and found that 61% (19/31) neurons showed increased firing rates to both itch-scratching and nociceptive stimuli (Figure 1H). These results indicate that VB neuronal activities are correlated with both scratching behavior and pain-related behavior.

The effects of manipulation of VB activity on pruritogens-induced scratching behaviors

To determine the functional role of VB in itch signal processing, we first employed a chemogenetic method of designer receptors exclusively activated by designer drugs (DREADDs). We injected AAV encoding the inhibitory DREADD receptor hM4Di fused with mCherry (AAV-hSyn-hM4Di-mCherry) into the VB (Figures 2A and S3A). The control group was injected with AAV-hSyn-mCherry. We verified the efficiency of silencing VB neurons expressing hM4Di in acute brain slices and found that bath application of clozapine-*N*-oxide (CNO, 5 μM) hyperpolarized the hM4Di^{+} neurons (Figures S3B and S3C). Then, we examined the pruritogens-induced scratching behaviors 30 minutes after the intraperitoneal injection of CNO (1 mg/kg). The inhibition of VB neurons significantly suppressed scratching behaviors induced by histamine or chloroquine (Figures 2B–2E) without significantly affecting locomotion activity (Figures S6A–S6C).

Using AAV-hSyn-hM4Di-mCherry virus might also inhibit very few GABAergic neurons in the VB and nearby TRN. We next specifically manipulate the excitatory neurons in the VB by using the *VGlut2-ires-Cre* mice. We injected a Cre-dependent AAV encoding *Gt*ACR1 (AAV-CAG-DIO-*Gt*ACR1-EGFP) into the VB of

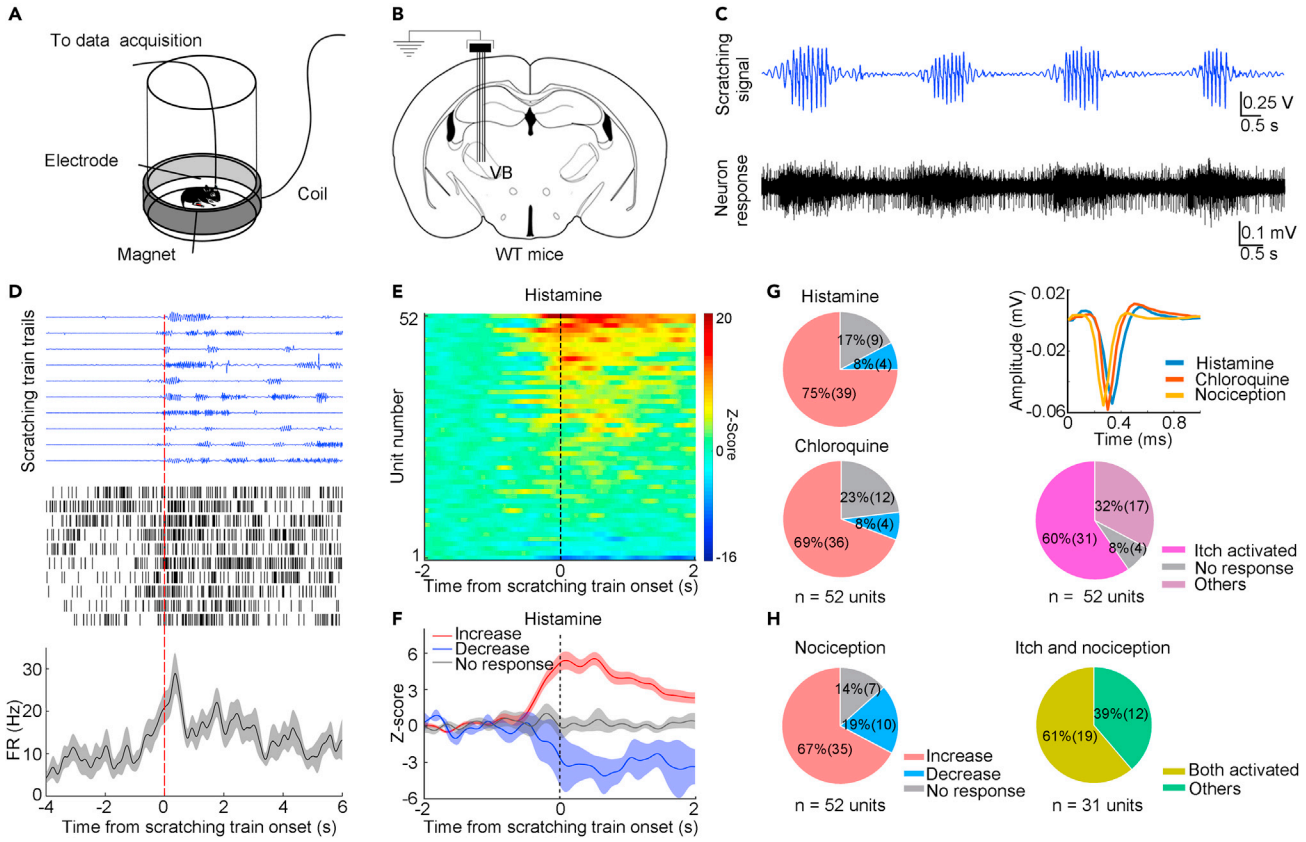

Figure 1. Dynamics of the VB Neurons during Pruritogens-Induced Scratching Behaviors and Nociceptive Mechanical Stimulus

(A) Schematic for recording neuronal activity and scratching behavior simultaneously.

(B) The implantation of a multielectrode array in the VB.

(C) A showcase of scratching signal (top) and neuronal activity (bottom).

(D) An example unit showing increased firing rates at the scratching train onset in response to histamine. Top, scratching trains aligned to the onset; Middle, spike raster with each row corresponding to a single scratching trial; Bottom, averaged firing rate (FR) across trials with shaded area indicating SD.

(E) Heatmap of activity of VB units in response to histamine, each row represents one unit (n = 52 units).

(F) Averaged Z-scored firing rates for units with significantly increased and decreased activities and those that showed no significant change in response to histamine (pre-scratching versus post-scratching train onset, red, *p < 0.05, blue, *p < 0.05, gray, p > 0.05, Wilcoxon signed-rank test). Shaded area indicated SD.

(G) Upper right: Average waveforms of a representative unit recognized in histamine, chloroquine, and nociceptive mechanical tests; Upper left: Percentage of units based on the activity in response to histamine (n = 52 units); Lower left: Percentage of units based on the activity in response to chloroquine (n = 52 units); Lower right: Percentage of units based on the activity in response to both histamine and chloroquine (increase/itch activated, n = 52 units).

(H) Left: Percentage of units based on the activity in response to nociceptive mechanical stimulus (n = 52 units); Right: Percentage of units based on the activity in response to both itch and nociceptive mechanical stimuli (n = 31 units).

VGlut2-ires-Cre mice (Figure S4A). We also verified the efficiency of silencing VB neurons via a 473 nm laser (Figures S4B and S4C). We found that the optogenetic inhibition of VB excitatory neurons decreased histamine- or chloroquine-induced scratching behaviors (Figures S4D–S4G) without significantly affecting locomotion activity (Figures S6G and S6H).

Next, we wondered whether the activation of VB excitatory neurons is sufficient to facilitate itch-induced scratching behaviors. To answer this question, we injected AAV-Ef1α-DIO-hM3Dq-mCherry or AAV-Ef1α-DIO-mCherry into the VB of *VGlut2-ires-Cre* mice (Figures 2F and S3D). We verified the efficiency of activation of VB neurons in brain slices (Figures S3E and S3F). We found that activation of VB excitatory neurons did not induce spontaneous scratching (30 minutes, Figures S5A and S5B) but significantly facilitated histamine-induced or chloroquine-induced scratching behaviors (Figures 2G–2J) without affecting locomotion activity (Figures S6D–S6F). These results indicate that activation of VB excitatory neurons is sufficient to facilitate pruritogens-induced scratching behaviors.

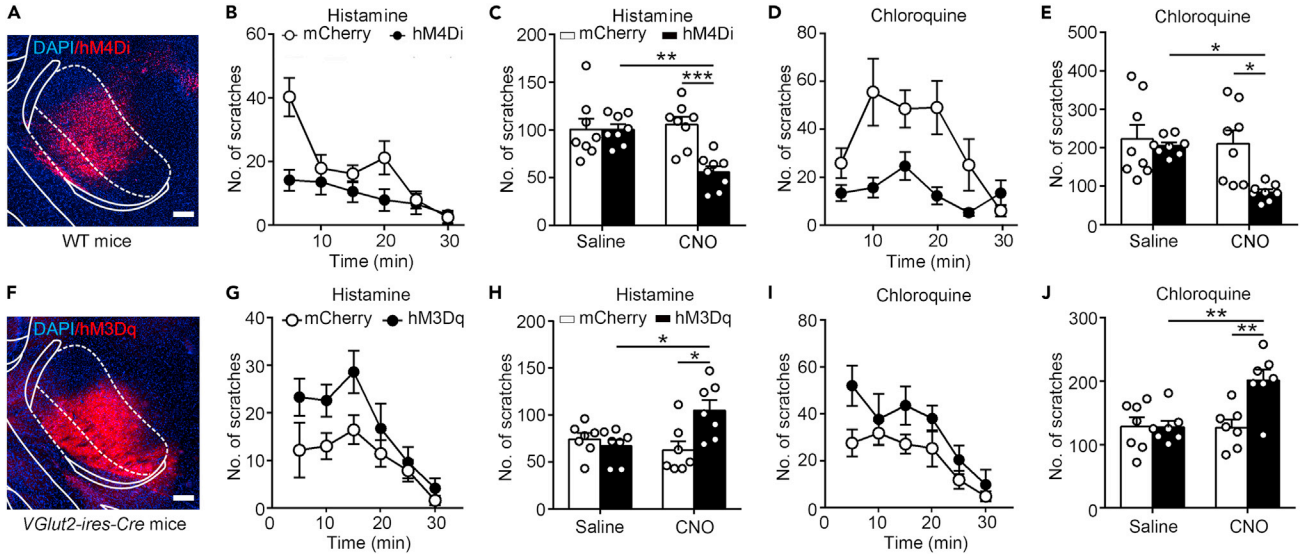

Figure 2. The Effect of Manipulation of VB Activity on the Pruritogens-Induced Scratching Behaviors

(A) Histological verification of the hSyn-hM4Di-mCherry expression in the VB of the wild type mice. Scale bar, 200 μm.

(B–E) Time course and summary of histamine-induced (B and C) or chloroquine-induced (D and E) scratching behaviors after CNO injection (n = 8 mice for each group, 1 mg/kg CNO, i.p.). *p < 0.05, **p < 0.01, ***p < 0.001, two-way ANOVA analysis followed by Bonferroni *post hoc* analysis.

(F) Histological verification of the DIO-hM3Dq-mCherry expression in the VB of the *VGlut2-ires-Cre* mice. Scale bar, 200 μm.

(G–J) Chemogenetic activation of VB glutamatergic neurons facilitated histamine-induced or chloroquine-induced scratching behaviors (n = 7 mice for each group). Time course and summary of histamine-induced (G and H) or chloroquine-induced (I and J) scratching behavior after CNO administration (1 mg/kg, i.p.). *p < 0.05, **p < 0.01, two-way ANOVA analysis followed by Bonferroni *post hoc* analysis. Data are presented as mean ± SEM.

The effects of manipulation of VB activity on basal nociception and pathological pain behaviors

Next, we measured the paw withdrawal responses by von Frey and Hargreaves tests to examine whether manipulation of VB affects the basal nociception. We found that inhibition or activation of VB activity did not affect the basal nociceptive thresholds (Figures 3A–3D, S6I, and S6J). We further examined the role of VB in pathological pain. We employed the optogenetic method to suppress the VB activity by injecting AAV-DIO-eNpHR3.0-EGFP and implanting the optical fiber in the VB of the *VGlut2-ires-Cre* mice. We found that optogenetic inhibition of the VB could significantly relieve spared nerve injury (SNI)-induced neuropathic pain and formalin-induced inflammatory pain (Figures 3E–3L). These results indicate that inhibition of VB could relieve pathological pain.

The TRN-VB inhibitory projections are involved in itch and pain signals processing

To further dissect the neural circuit that modulates VB, we used a retrogradely transported AAV (retroAAV) to label VB-projecting brain areas (Tervo et al., 2016). We injected retroAAV-hSyn-Cre into the VB of *Rosa26-tdTomato* mice (Figures 4A and 4B). We found that neurons were mainly labeled in the adjacent ventral TRN (Figures 4C–4E), ipsilateral somatosensory cortex, and other nuclei. It has been reported that TRN neurons provide topographic inhibition to thalamic relay cells (Lam and Sherman, 2007; Pinault and Deschnes, 1998). Furthermore, we injected AAV-Ef1α-DIO-EGFP into the dorsal TRN or ventral TRN, respectively (Figures 4F and 4K), and dissected its projection fibers. We found that the dorsal TRN predominantly projected to the posterior thalamic nucleus (Po), with a few projection fibers to the ventrolateral part of the laterodorsal thalamus (LDVL) and the mediorostral part of the lateral posterior thalamus (LPMR, Figures 4G–4J), whereas the ventral TRN mainly innervated the VB (Figures 4L–4O).

We then verified the synaptic characteristics of TRN-VB projection. We injected AAV-Ef1α-DIO-ChR2-mCherry into the TRN neurons and found that 473 nm laser pulses induced reliable action potentials in ChR2 positive TRN neurons (Figures 4P–4R). Recording from VB neurons, we found that photostimulation of TRN-VB projections induced short-latency inhibitory postsynaptic currents (IPSCs) (21 of 24 neurons recorded, Figures 4S and 4T), which were blocked by the $GABA_A$ receptor antagonist picrotoxin (PTX). The

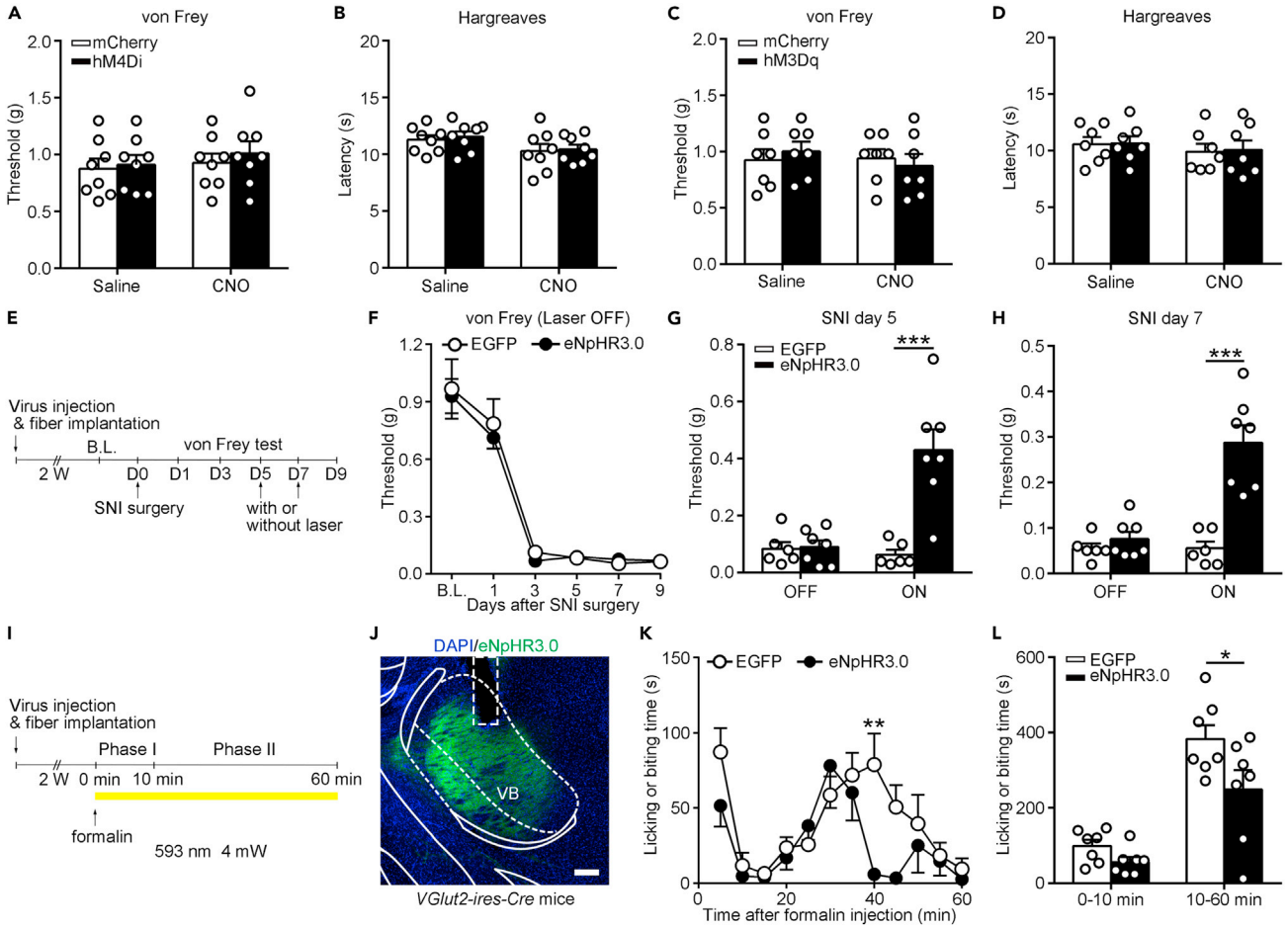

Figure 3. The Effects of Manipulation of VB Activity on Basal Nociception and Pathological Pain

(A and B) Chemogenetic inhibition of VB activity did not affect basal paw withdrawal threshold (A) and basal paw withdrawal latency (B) tested by von Frey or Hargreaves tests (n = 8 mice for each group).

(C and D) Chemogenetic activation of VB had no effect on basal paw withdrawal threshold (C) and basal paw withdrawal latency (D) tested by von Frey or Hargreaves tests (n = 7 mice for each group).

(E) Timeline of the SNI-induced neuropathic pain experiments.

(F) SNI-induced hyperalgesia-like symptoms in AAV-EGFP group and AAV-eNpHR3.0 group (EGFP group, n = 6 mice; eNpHR3.0 group, n = 7 mice).

(G and H) The mechanical paw withdrawal threshold during laser ON (593 nm, 4 mW) or laser OFF phase at day 5 (G) and day 7 (H) after SNI surgery. ***$p < 0.001$; two-way ANOVA analysis followed by Bonferroni *post hoc* analysis.

(I) Timeline of the formalin-induced inflammatory pain experiments.

(J) Histological confirmation of the virus infection and optical fiber location. The rectangle indicated the optical fiber location. Scale bar, 200 μm.

(K) Licking or biting time after formalin injection in a 5-minute interval in AAV-EGFP group and AAV-eNpHR3.0 group (n = 7 mice for each group). **$p < 0.01$. Two-way repeated ANOVA analysis followed by Bonferroni *post hoc* analysis.

(L) Cumulative licking or biting time during phase I (0–10 min) and phase II (10–60 min). *$p < 0.05$. two-way ANOVA analysis followed by Bonferroni *post hoc* analysis. Data are presented as mean ± SEM.

average amplitude of the light-evoked IPSCs of 21 neurons was 621.2 ± 106.6 pA (Figure S7A). The latency of light-induced IPSCs was 2.981 ± 0.155 ms with short jitter (0.216 ± 0.029 ms, Figures S7B and S7C), indicating a monosynaptic GABAergic connection between TRN neurons and VB neurons. We also confirmed that there were no obvious light-induced excitatory postsynaptic currents (EPSCs).

To determine whether TRN-VB projections are involved in itch signal processing, we first examine the calcium activity of the TRN neurons. We injected AAV-Ef1α-DIO-GCaMP6s and implanted optical fibers into the TRN of *Vgat-ires-Cre* mice (Figure 5A). We observed elevated fluorescence signals during scratching trains, indicating that the calcium activity of these neurons was increased during scratching behavior (Figures 5B–5E). Furthermore, we injected AAV-Ef1α-DIO-GCaMP6s into the TRN and implanted optical

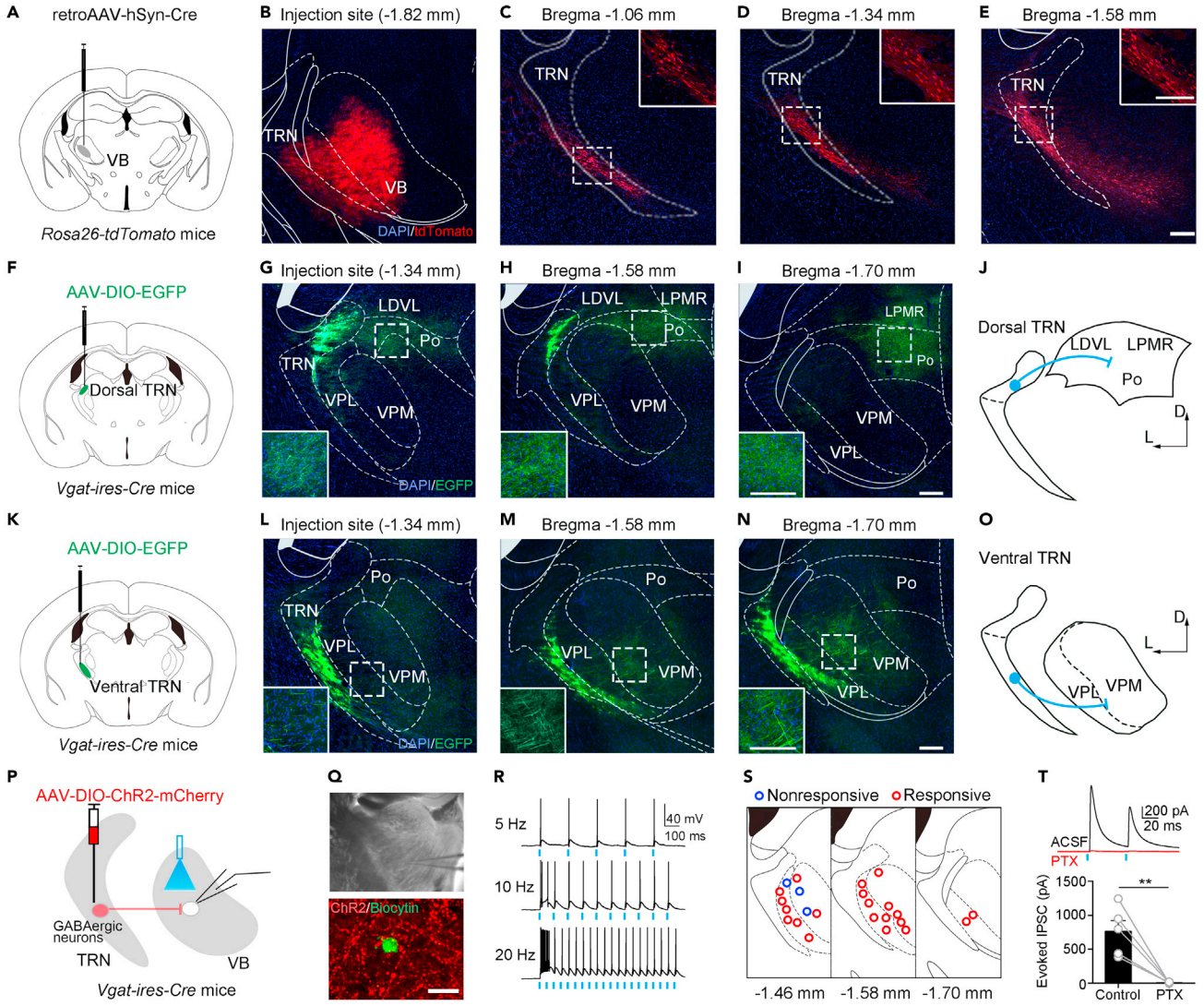

Figure 4. The VB Mainly Receives the Ventral TRN Inhibitory Projections

(A) Schematic of the virus injection into the VB of the *Rosa26-tdTomato* mice.

(B) Histological verification of the virus infection.

(C–E) Representation of retrogradely labeled neurons on distinct coronal sections of TRN. Images were magnified in solid white rectangles. Scale bars, 200 μm.

(F) Schematic showing virus injection into dorsal TRN.

(G–I) Virus expression area in dorsal TRN and the projection fibers in the posterior thalamus (Po), ventrolateral part of the laterodorsal thalamus (LDVL), and mediorostral part of the lateral posterior thalamus (LPMR) on distinct coronal sections. Scale bars, 200 μm.

(J) Schematic diagram of dorsal TRN projection pattern. D, dorsal; L, lateral.

(K) Schematic showing virus injection into ventral TRN.

(L–N) Virus expression area and the projection fibers in the VB. Scale bars, 200 μm.

(O) Schematic diagram of ventral TRN projection pattern. D, dorsal; L, lateral.

(P) Schematic of virus injection in the TRN and recording configuration in acute slices.

(Q) Top: Bright field inverted microscope image of recording in the VB neurons. Bottom: Image showing biocytin staining of a recording neuron (green) and $ChR2^+$ fibers (red), scale bar, 50 μm.

(R) 473 nm laser-induced time-locked action potential firing at 5 Hz, 10 Hz, and 20 Hz in a representative TRN $ChR2^+$ neuron. Scale bars, 100 ms, 40 mV.

(S) The locations of 24 recorded neurons in the VB.

(T) The light-evoked IPSCs were completely blocked by 100 μM PTX (picrotoxin, top). Summary of the amplitude of light-evoked IPSCs (bottom). Paired two-sided t test, $^{**}p < 0.01$ (n = 5 neurons). Data are presented as mean ± SEM.

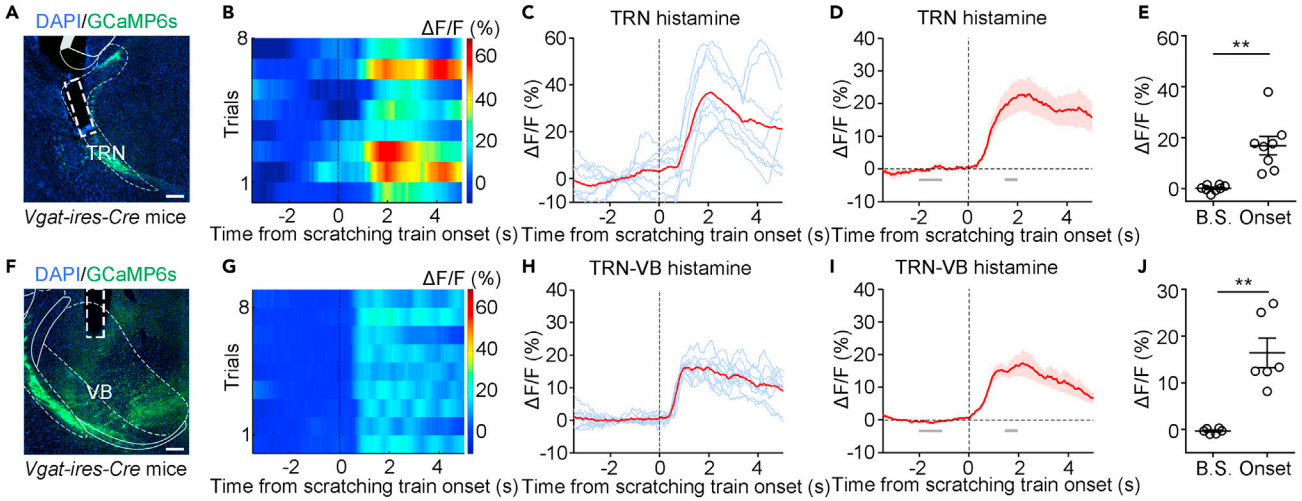

Figure 5. The Calcium Signal of TRN Neurons and TRN-VB Inhibitory Projections during Histamine-Induced Scratching Behavior

(A–E) The calcium signal of TRN neurons during the histamine-induced scratching behaviors. (A) The histological verification of the virus infection and the optical fiber site in the TRN. Scale bar, 200 μm. (B) An example of heatmap illustrating Ca^{2+} transients of a mouse aligned to the onset of each scratching train. (C) Individual trial (blue) and the mean Ca^{2+} transients (red) across different scratching trails of a mouse. (D) Mean calcium signal of the TRN neurons in response to histamine, the gray scale bars represent the baseline (−2 s to −1 s, B.S.) and the onset (1.5 s–2 s, Onset). (E) Quantification of mean calcium signal change during the two periods (n = 8 mice, paired two-sided t test, **$p < 0.01$).

(F–J) The calcium signal of TRN-VB projections during the histamine-induced scratching behavior. (F) The histological verification of the virus injection and the optical fiber site. Scale bar, 200 μm. (G) An example of heatmap illustrating Ca^{2+} transients of a mouse aligned to the onset of each scratching train. (H) Individual trial (blue) and the mean Ca^{2+} transients (red) across different scratching trails of a mouse. (I) Mean calcium signal of the TRN-VB projections in response to histamine, the gray scale bars represent the baseline (−2 s to −1 s, B.S.) and the onset (1.5 s–2 s, Onset). (J) Quantification of mean calcium signal change during the two periods (n = 6 mice, paired two-sided t test, **$p < 0.01$). Data are presented as mean ± SEM.

fibers into the VB of *Vgat-ires-Cre* mice to record the calcium signal of TRN-VB projections (Figure 5F). We found that VB-projecting fibers displayed a similar increase in calcium activity during histamine-induced scratching behavior (Figures 5G–5J). Besides, we compared the calcium signals of the VB, TRN neurons, and TRN-VB projections, and the calcium signal change in VB neurons was significantly increased at the onset point (−0.2 s–0.2 s), whereas the calcium signal change in TRN neurons and projection fibers at this point was close to zero (Figure S8). Moreover, we also found that the calcium activity of TRN-VB projections was elevated in response to the pinch stimulus applied on the neck or the tail (Figure S9). These results indicated that TRN-VB projections are involved in itch and pain signals processing.

Functional role of TRN-VB projections in itch processing

We speculated that activation of TRN-VB inhibitory projections would suppress VB and disturb itch processing. We injected AAV-Ef1α-DIO-ChR2-mCherry into TRN and implanted optical fiber into the VB (Figures S10A and S10B). The optogenetic activation of TRN-VB projections significantly suppressed histamine-induced or chloroquine-induced scratching behavior without affecting the locomotor activity (Figures 6A–6D, S10C, and S10D). To further demonstrate the functional role of the TRN, we then ablated TRN GABAergic neurons by a taCaspase3-based method (Yang et al., 2013). We injected AAV-CAG-DIO-taCaspase3-TEVp into TRN of *Vgat-ires-Cre* mice with AAV-Ef1α-DIO-EGFP as the control (Figure 6E). Four weeks later, mice injected with AAV-CAG-DIO-taCaspase3-TEVp showed very few $NeuN^+$ (a neuronal marker) neurons in the TRN, compared with mice injected with the control virus (Figures 6F and 6G). We also verified the ablation areas of TRN along the anterior-posterior axis (Figure S11). Ablation of the TRN significantly exacerbated the scratching behaviors induced by histamine or chloroquine and did not affect the locomotion or the weight of the mice (Figures 6H, 6I, S10E, and S10F). These results indicate that TRN-VB projections play a key role in modulating itch signal processing.

The effect of manipulation of TRN-VB projections on basal nociception and pathological pain behaviors

We further examined the effect of manipulation of TRN-VB projections on the basal nociception and found that the activation of TRN-VB or the ablation of TRN did not affect the basal nociception (Figures 7A–7D).

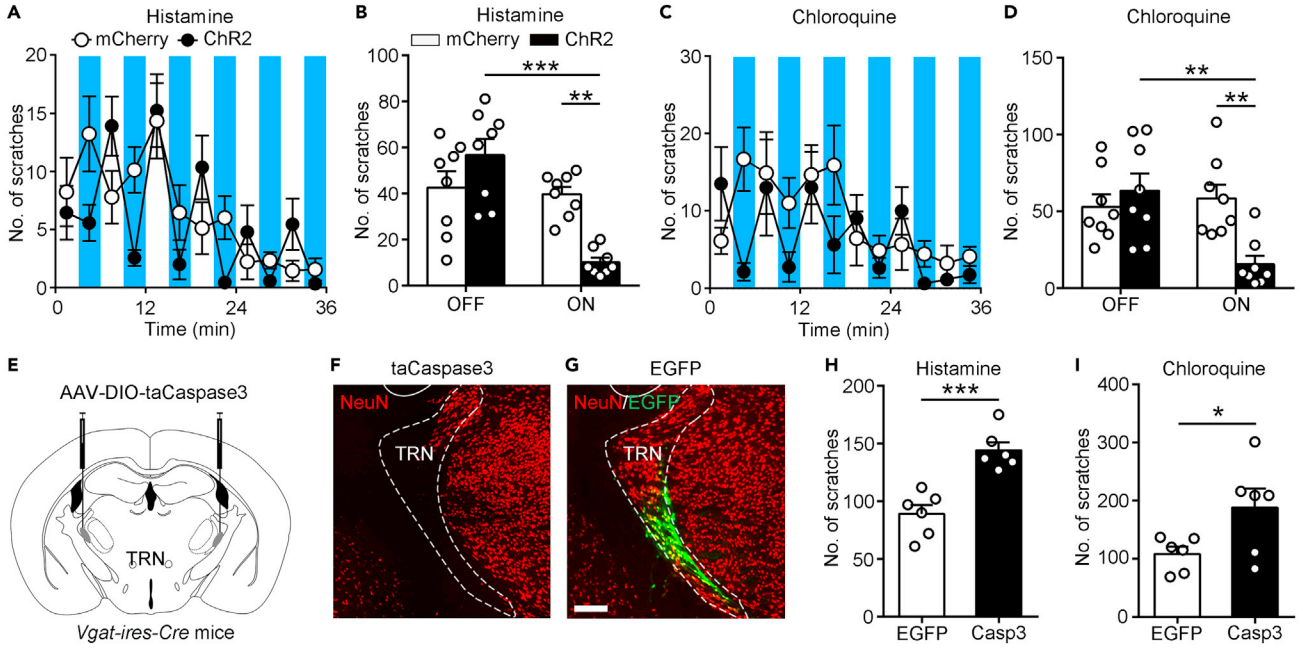

Figure 6. The Effects of Activation of TRN-VB Inhibitory Projections or Ablation of TRN on the Pruritogens-Induced Scratching Behaviors

(A–D) Optogenetic activation of TRN-VB inhibitory projections relieved the scratching behaviors. Time course and summary of histamine-induced (A and B) or chloroquine-induced (C and D) scratching behaviors during optogenetic activation of TRN-VB projections. Each point in (A) and (C) represents the number of scratching bouts in a 3-minute laser-OFF/ON period (473 nm, 4 mW, 20 Hz, blue shaded). **p < 0.01, ***p < 0.001. two-way ANOVA analysis followed by Bonferroni *post hoc* analysis (n = 8 mice for each group).

(E) Schematic showing virus injection.

(F and G) NeuN staining in taCaspase3 group and EGFP group. Scale bar, 200 μm.

(H and I) Ablation of TRN enhanced scratching behaviors in response to histamine and chloroquine (n = 6 mice per group). *p < 0.05, ***p < 0.001. Unpaired two-sided t test. Data are presented as mean ± SEM.

Then, we wondered whether the TRN-VB projections regulate pathological pain. We found that optogenetic activation of TRN-VB projections significantly relieved the neuropathic pain symptom in the SNI model (Figures 7E–7G). Furthermore, activation of the TRN-VB projections significantly reduced the licking or biting time, especially in the second phase of formalin pain (Figures 7H–7J). These results indicate that TRN-VB projections also modulate pathological pain.

DISCUSSION

In this study, we demonstrated a local thalamic circuit involved in itch and pain signals processing. Most of the VB neurons recorded were activated in response to pruritic and nociceptive stimuli. Manipulation of the VB or the TRN-VB projections modulated itch-related and pain-related behaviors.

Neuronal activity of the VB during itch and pain signals processing

The coding of distinct modalities, including itch and pain, is a synergistic theory that involves both the specificity theory (labeled line) and the crosstalk theory (Craig, 2003; Ma, 2010). Whether itch and pain activate the same population of neurons in the thalamus is still a critical question. Previous extracellular recording studies in anesthetized animals have shown that most of the spinothalamic neurons, trigeminothalamic neurons, thalamic neurons, and primary somatosensory cortex neurons are activated in both itch and pain (Davidson et al., 2012; Khasabov et al., 2020; Lipshetz et al., 2018; Moser and Giesler, 2014). In our study, we performed extracellular recording on free-moving mice and examined the neuronal activity in response to itch and pain stimuli. We found that most VB neurons responsive to the pruritic-induced scratching behaviors could also be activated during mechanical nociceptive stimulus-induced withdrawal behaviors. One reason for the high portion of the co-activated neurons could be that itch-induced scratching behavior also induced robust mechanical inputs. Another reason could be that VB neurons might process distinct modalities, including chemical itch sensation and mechanical nociception sensation. Lipshetz

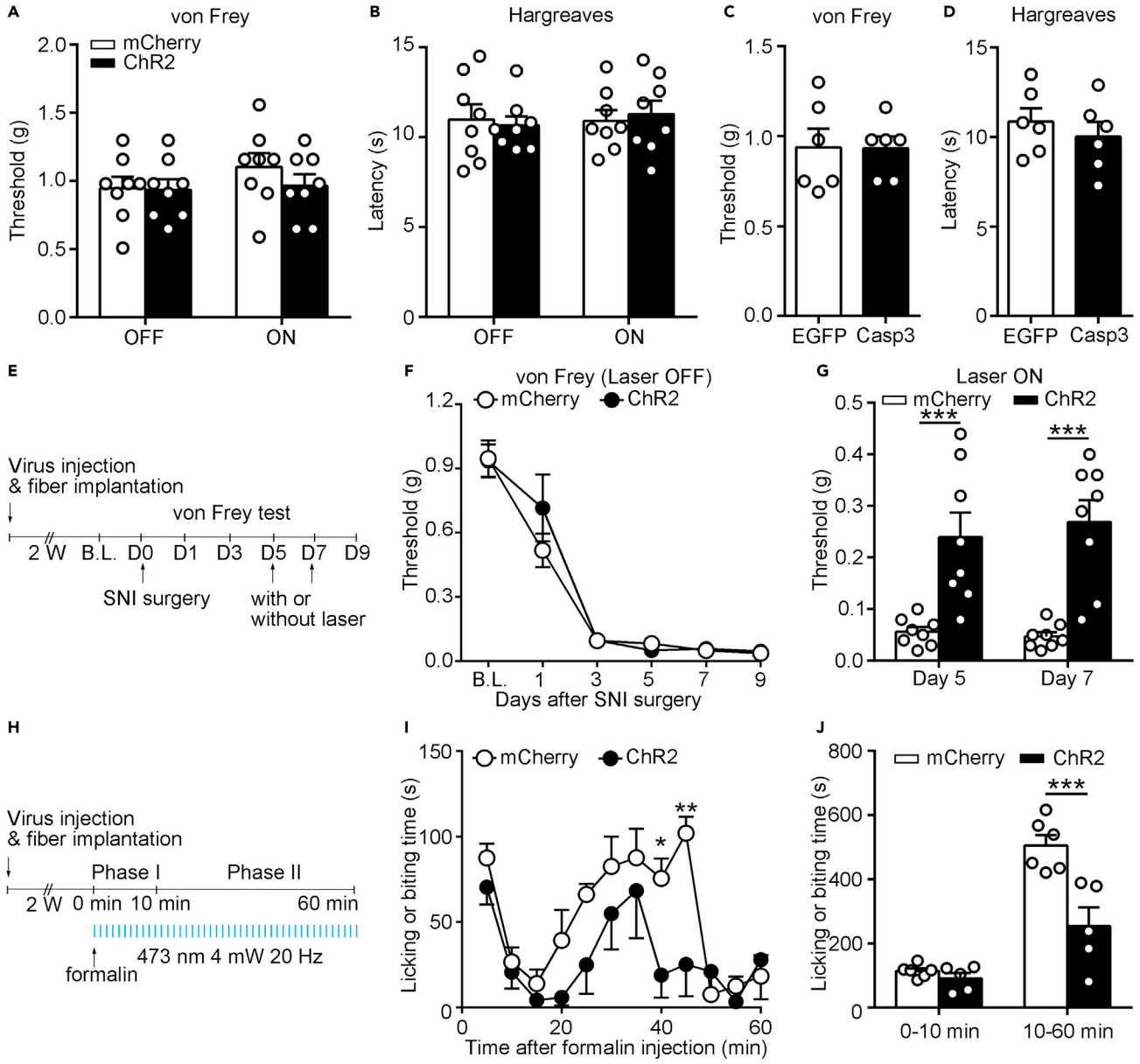

Figure 7. The Effect of Manipulation of TRN-VB Inhibitory Projections on Basal Nociception and Pathological Pain

(A and B) Optogenetic activation of TRN-VB projections had no effect on the basal paw withdrawal responses tested by von Frey (A) and Hargreaves (B) tests, respectively (n = 8 mice for each group).

(C and D) Ablation of TRN had no effect on the basal paw withdrawal responses tested by von Frey (C) and Hargreaves (D) tests, respectively (n = 6 mice for each group).

(E) Timeline of the SNI-induced neuropathic pain experiments.

(F) SNI-induced hyperalgesia-like symptoms in AAV-mCherry group and AAV-ChR2 group (n = 8 mice for each group).

(G) The paw withdrawal threshold during laser ON (473 nm, 4 mW, 20 Hz) at day 5 and day 7 after SNI surgery. ***$p < 0.001$; two-way ANOVA analysis followed by Bonferroni *post hoc* analysis.

(H) Timeline of the formalin-induced inflammatory pain experiments.

(I) Licking or biting time after formalin injection in 5-minute intervals during activation of TRN-VB projections in mCherry group and ChR2 group (n = 8 mice for each group). *$p < 0.05$, **$p < 0.01$. Two-way repeated ANOVA analysis followed by Bonferroni *post hoc* analysis.

(J) Cumulative licking or biting time with optogenetic activation of TRN-VB inhibitory projections during phase I (0–10 minutes) and phase II (10–60 minutes) in mCherry group and ChR2 group. ***$p < 0.001$. two-way ANOVA analysis followed by Bonferroni *post hoc* analysis. Data are presented as mean ± SEM.

et al. showed that about 80% of nociceptive thalamic neurons were responsive to pruritogens in anesthetized rats, which did not have scratching-induced mechanical inputs (Lipshetz et al., 2018). In addition, the ventral anterior thalamus (VA) and ventral lateral thalamus (VL) are involved in motor functions (Bosch-Bouju et al., 2013). The VB is laterally positioned to the VL and is thought to be mainly involved in sensation transmission. Whether the VB also participates in motor planning or execution needs further examination.

Although the portion of itch and pain co-activated neurons was high in our study, there still might be specific neurons or circuits in the VB that differentially transmit itch or pain sensory. Further RNA-sequencing techniques combined with targeted combination in active populations (TRAP) method might provide potential molecular information of itch-specific and pain-specific populations in the thalamus (Guenthner et al., 2013; Samineni et al., 2021). Another way is using the recently developed CaRMA (calcium and RNA multiplexed activity) imaging platform, which could monitor the calcium dynamics of multiple molecularly defined cell types in parallel, within a deep-brain region, and across various behaviors (Xu et al., 2020). Further genetic deletion of specific subpopulations by the Diphtheria toxin system might dissect its roles in itch and pain. Such state-of-the-art strategies might help to develop a detailed classification of VB neurons.

Another critical question is whether VB neurons distinguish histaminergic versus nonhistaminergic itch. Extracellular recordings studies reported that some spinothalamic tract (STT) neurons responded to histamine or cowhage (non-histaminergic dependent pruritogen), respectively (Davidson et al., 2007, 2012). Lipshetz et al. examined the response of 66 thalamic neurons to itch- and pain-inducing stimuli, including chloroquine, serotonin, β-alanine, histamine, and capsaicin in rats (Lipshetz et al., 2018). Forty percent of these neurons responded to the injection of three, four, or even five agents. They also found no significant differences in coefficient of variation or interspike interval distributions in firing patterns within the responses of thalamic neurons to various agents. Consistently, we found that more than half of the neurons recorded in VB responded to both histamine and chloroquine. The majority of VB neurons that responded to pruritogens might converge multiple types of itch information and encode a topography of location and intensity rather than specifically transmit individual agents discriminately. However, the hypothesis that a subpopulation of VB neurons specifically responds to histaminergic or nonhistaminergic stimuli cannot be rejected based on current results.

Functional role of VB in itch and pain

The spinothalamic pathway and the spinoparabrachial pathway are two major ascending pathways from the spinal cord. Recent studies have found that the PBN-related circuits play critical roles in itch-related behavior, nocifensive behavior (Deng et al., 2020; Mu et al., 2017; Samineni et al., 2021; Sanders et al., 2019), anxiety, fear, or aversion (Chiang et al., 2019), supporting that the spinoparabrachial tract and the PBN are involved in the emotional component of pain (Basbaum et al., 2009) and itch signal processing.

The thalamus is considered to be an important center in processing the sensory component of itch and pain sensations. Lipshetz et al. found that about 80% (27/34) of ventroposteromedial (VPM) neurons were pruriceptive (Lipshetz et al., 2018). The posterior triangular nucleus (PoT), a high-order thalamic nucleus (Halassa and Sherman, 2019) has also been shown to be a facial itch-responsive nucleus (Lipshetz et al., 2018; Zhu et al., 2020). A few studies in rodents and primates performed lesion experiments to explore the functional role of the VB in pain processing. One study showed that hemorrhagic lesion within the ventroposterolateral thalamus (VPL) could lead to mechanical allodynia and thermal hyperalgesia (Nagasaka et al., 2017), whereas another study showed lesion or blockage of the VB attenuated neuropathic pain (Saade et al., 2006). There is still a lack of systematic studies on the functional role of the VB in itch and pain.

In our study, we first examined the functional role of the VB by performing optogenetic and chemogenetic manipulation. We found that inhibition of the VB relieved the scratching behaviors and activation of VB facilitated the scratching behaviors in histamine and chloroquine experiments. Furthermore, we found that transient manipulation of the VB did not disturb basal nociception but partially relieved the SNI-induced and formalin-induced pain. Previous studies have found that spinal cord injury-induced long-term potentiation (LTP) in thalamic neurons (Gerke et al., 2003; Hains et al., 2006; Luo et al., 2014). We speculate that the VB might be activated abnormally or enhanced synaptic plasticity in the SNI- or formalin-induced pain, and inhibition of VB activity could attenuate the pain-related behaviors. It is noteworthy that we performed chemogenetic manipulations of VB bilaterally and optogenetic manipulation contralaterally. According to the contralateral projection

of the spinothalamic tract, we speculate that the contralateral VB is mainly involved in itch and pain processing. It should also be noted that we used different optogenetic tools to inhibit the VB and both tools are well-recognized. The *Gt*ACR1 is a blue light-activated anion channel, and the eNpHR3 is a yellow light-driven chloride pump. The most important advantage of the *Gt*ACR1 is that the 473 nm laser (commonly for ChR2 experiments) could activate it, making it convenient for performing both inhibition and activation experiments by the same equipment system.

TRN-VB projections modulate itch and pain

Thalamic inhibition is a critical element of thalamic projection neurons interactions, and evidence for its perturbation is found in many diseases, including both pain and itch (Halassa and Acsady, 2016; Steinhoff et al., 2018). Recent studies have also identified that the posterior thalamic nucleus (Po) and the zona incerta-Po inhibitory projection modulate nocifensive behaviors (Wang et al., 2020; Zhu et al., 2021). Most VB neurons are excitatory neurons, and the best-studied source of VB inhibition is derived from the TRN (Halassa and Acsady, 2016). An early study found that the TRN lesion enlarges the average receptive field of VPM neurons and increases the average response (probability and magnitude) of the center receptive field whisker in rats (Lee et al., 1994). Other researchers found that the TRN-VB projections contribute to chronic inflammatory pain (Potes et al., 2006; Zhang et al., 2017).

Recently, a study reported hierarchical connectivity between TRN and distinct thalamic nuclei. The core region of TRN projects to first-order thalamic nuclei, including somatosensory thalamic nuclei, and the shell region of TRN projects to the high-order thalamic nuclei (Li et al., 2020). Another research reported that the dorsal TRN projects to the anterior thalamic nuclei and laterodorsal thalamic nucleus (LD) (Halassa et al., 2014). In our study, we performed tracing experiments and found that the dorsal TRN mainly projects to Po, LDVL, and LPMR. The ventral TRN predominantly projects to the VB along the anterior-posterior axis. Our results enriched the understanding of a comprehensive architecture of the TRN-thalamic nuclei connectivity. Next, the calcium recording results showed that the calcium activity of the VB-projecting fibers was elevated during itch-induced scratching behaviors and pinch stimulus. Notably, the calcium signal change in VB neurons was significantly increased at the onset point (−0.2 s–0.2 s), whereas the calcium signal change in TRN neurons and projection fibers at this point was close to zero. The time differences between VB neurons with TRN neurons and TRN-VB projections might be explained as itch sensation initially elevates the activity of VB and the mouse begins to scratch after the activity reaches the threshold, then the itch sensation and scratching behaviors lead to prolonged elevated calcium signal in VB and TRN. We speculate that the activation of TRN-VB inhibitory projections would suppress VB to prevent excessive activation (negative feedback loop). Then we found that the selective activation of TRN-VB inhibitory projections suppressed pruritogens-induced scratching behaviors. This data was consistent with the result of the inhibition of VB with optogenetic or chemogenetic manipulation. We further found that ablation of TRN facilitated itch behavior without affecting motor ability. In addition, we found that activation of TRN-VB projections had analgesic effects on both SNI-induced and formalin-induced pain without affecting the basal nociceptive threshold. This is consistent with a previous study that showed activation of TRN-VB projections could relieve Freund's adjuvant-induced inflammatory pain completely (Zhang et al., 2017). These data suggest that the TRN-VB inhibitory projections play a critical role in modulating pathological pain.

Notably, recent studies showed distinct neuron types and circuits in the TRN (Clemente-Perez et al., 2017; Li et al., 2020; Martinez-Garcia et al., 2020). The calbindin-expressing neurons located in the central core and connect with the VB (Martinez-Garcia et al., 2020). An integrative study showed that *Spp1* (encoding secreted phosphoprotein 1)-expressing neurons mainly project to first-order thalamic nuclei, including the VPM and VPL (Li et al., 2020). Whether these VB-projecting TRN neurons respond to itch and pain differentially needs further research.

In conclusion, the present study supports a hypothesis that VB is involved in both itch and pain signals processing. Manipulation of the VB or the TRN-VB inhibitory projections modulates both itch and pain. Enhancing the inhibitory tone in the ascending pathway might be a potential strategy for treating chronic itch and pain.

Limitations of the study

Detailed molecular information of itch- and pain-related populations in the VB should be further dissected with the RNA-sequencing technique method. In addition, the *Spp1* (encoding secreted phosphoprotein 1)-expressing neurons in TRN have been reported to be mainly projecting toward first-order thalamic nuclei,

including the VB. Whether these neurons respond to itch and pain differentially needs further research. Furthermore, whether there are plasticity changes in the TRN-VB projections during chronic itch and pain is still elusive.

STAR★METHODS

Detailed methods are provided in the online version of this paper and include the following:

- KEY RESOURCES TABLE
- RESOURCE AVAILABILITY
  - Lead contact
  - Materials availability
  - Data and code availability
- EXPERIMENTAL MODEL AND SUBJECT DETAILS
- METHOD DETAILS
  - General surgical procedures and viral delivery
  - Surgery for injection into VB
  - Surgery for injection into TRN
  - Implantation of optical fibers in the VB or TRN
  - Fiber photometry
  - Itch behavior test
  - Analysis of the scratching behaviors
  - Nociceptive behavior
  - Spared nerve injury model
  - Formalin test
  - Open field test
  - Rotarod
  - Chemogenetic manipulations
  - Optogenetic manipulations
  - Brain slice electrophysiology
  - Immunohistochemical staining
  - Extracellular recording
- QUANTIFICATION AND STATISTICAL ANALYSIS

SUPPLEMENTAL INFORMATION

Supplemental information can be found online at https://doi.org/10.1016/j.isci.2021.103625.

ACKNOWLEDGMENTS

We thank Yan-Gang Sun and Xing-Jun Liu for their comments on the manuscript. We thank Yan-Gang Sun and Hua-Tai Xu for providing *VGlut2-ires-Cre*, *Vgat-ires-Cre*, and *Rosa26-tdTomato* mice. We thank Lei Yuan, Yan Jing Zhu for their technical support. This work was supported by National Natural Science Foundation of China (No. 31900717, 31571086), the Shanghai Sailing Program from Shanghai Association for Science and Technology (19YF1438700, to D.M.), Youth talent support program from China Association for Science and Technology (2019QNRC001, to D.M.), Youth talent support program from Shanghai Jiao Tong University School of Medicine (19XJ11010, to D.M.), China Postdoctoral Science Foundation (2021M692451, to A.X.) and Starting Research Fund from the Shanghai General Hospital (to D.M.). We thank Enago (http://www.enago.com/) for the English language review.

AUTHOR CONTRIBUTIONS

P.-F.L., Y.W., and L.X. performed the virus injection experiments and behavioral experiments. A.-F.X. and X.J. performed the extracellular recording experiment. R.Z. performed the electrophysiological experiments. Y.-B.Z. and M.-Z.L. participated in the histological experiments. J.-B.L., L.Z., and D.M. designed the experiments. P.-F.L., L.Z., and D.M. wrote the manuscript.

DECLARATION OF INTERESTS

The manuscript has not been published previously, and is not under consideration for publication elsewhere. All authors declare that there are no competing financial interests in this study.

Received: August 17, 2021
Revised: November 16, 2021
Accepted: December 10, 2021
Published: January 21, 2022

REFERENCES

Basbaum, A.I., Bautista, D.M., Scherrer, G., and Julius, D. (2009). Cellular and molecular mechanisms of pain. Cell *139*, 267–284. https://doi.org/10.1016/j.cell.2009.09.028.

Bosch-Bouju, C., Hyland, B.I., and Parr-Brownlie, L.C. (2013). Motor thalamus integration of cortical, cerebellar and basal ganglia information: implications for normal and parkinsonian conditions. Front. Comput. Neurosci. *7*, 163. https://doi.org/10.3389/fncom.2013.00163.

Chen, X.J., and Sun, Y.G. (2020). Central circuit mechanisms of itch. Nat. Commun. *11*, 1–10. https://doi.org/10.1038/s41467-020-16859-5.

Chiang, M.C., Bowen, A., Schier, L.A., Tupone, D., Uddin, O., and Heinricher, M.M. (2019). Parabrachial complex: a hub for pain and aversion. J. Neurosci. *39*, 8225–8230. https://doi.org/10.1523/JNEUROSCI.1162-19.2019.

Clemente-Perez, A., Makinson, S.R., Higashikubo, B., Brovarney, S., Cho, F.S., Urry, A., Holden, S.S., Wimer, M., David, C., Fenno, L.E., et al. (2017). Distinct thalamic reticular cell types differentially modulate normal and pathological cortical rhythms. Cell Rep. *19*, 2130–2142. https://doi.org/10.1016/j.celrep.2017.05.044.

Craig, A.D. (2003). Pain mechanisms: labeled lines versus convergence in central processing. Annu. Rev. Neurosci. *26*, 1–30. https://doi.org/10.1146/annurev.neuro.26.041002.131022.

Davidson, S., Zhang, X., Khasabov, S.G., Moser, H.R., Honda, C.N., Simone, D.A., and Giesler, G.J., Jr. (2012). Pruriceptive spinothalamic tract neurons: physiological properties and projection targets in the primate. J. Neurophysiol. *108*, 1711–1723. https://doi.org/10.1152/jn.00206.2012.

Davidson, S., Zhang, X., Yoon, C.H., Khasabov, S.G., Simone, D.A., and Giesler, G.J., Jr. (2007). The itch-producing agents histamine and cowhage activate separate populations of primate spinothalamic tract neurons. J. Neurosci. *27*, 10007–10014. https://doi.org/10.1523/JNEUROSCI.2862-07.2007.

Deng, J., Zhou, H., Lin, J.K., Shen, Z.X., Chen, W.Z., Wang, L.H., Li, Q., Mu, D., Wei, Y.C., Xu, X.H., et al. (2020). The parabrachial nucleus directly channels spinal nociceptive signals to the intralaminar thalamic nuclei, but not the amygdala. Neuron *107*, 909–923. https://doi.org/10.1016/j.neuron.2020.06.017.

Dong, P., Wang, H., Shen, X.F., Jiang, P., Zhu, X.T., Li, Y., Gao, J.H., Lin, S., Huang, Y., He, X.B., et al. (2019). A novel cortico-intrathalamic circuit for flight behavior. Nat. Neurosci. *22*, 941–949. https://doi.org/10.1038/s41593-019-0391-6.

Dong, X.T., and Dong, X.Z. (2018). Peripheral and central mechanisms of itch. Neuron *98*, 482–494. https://doi.org/10.1016/j.neuron.2018.03.023.

Gao, Z.R., Chen, W.Z., Liu, M.Z., Chen, X.J., Wan, L., Zhang, X.Y., Yuan, L., Lin, J.K., Wang, M., Zhou, L., et al. (2019). Tac1-expressing neurons in the periaqueductal gray facilitate the itch-scratching cycle via descending regulation. Neuron *101*, 45–59.e9. https://doi.org/10.1016/j.neuron.2018.11.010.

Gauriau, C., and Bernard, J.-F. (2004). A comparative reappraisal of projections from the superficial laminae of the dorsal horn in the rat: the forebrain. J. Comp. Neurol. *468*, 24–56. https://doi.org/10.1002/cne.10873.

Gerke, M.B., Duggan, A.W., Xu, L., and Siddall, P.J. (2003). Thalamic neuronal activity in rats with mechanical allodynia following contusive spinal cord injury. Neuroscience *117*, 715–722. https://doi.org/10.1016/s0306-4522(02)00961-2.

Guenthner, C.J., Miyamichi, K., Yang, H.H., Heller, H.C., and Luo, L. (2013). Permanent genetic access to transiently active neurons via TRAP: targeted recombination in active populations. Neuron *78*, 773–784. https://doi.org/10.1016/j.neuron.2013.03.025.

Hains, B.C., Saab, C.Y., and Waxman, S.G. (2006). Alterations in burst firing of thalamic VPL neurons and reversal by Na(v)1.3 antisense after spinal cord injury. J. Neurophysiol. *95*, 3343–3352. https://doi.org/10.1152/jn.01009.2005.

Halassa, M.M., and Acsady, L. (2016). Thalamic inhibition: diverse sources, diverse scales. Trends Neurosci. *39*, 680–693. https://doi.org/10.1016/j.tins.2016.08.001.

Halassa, M.M., Chen, Z., Wimmer, R.D., Brunetti, P.M., Zhao, S., Zikopoulos, B., Wang, F., Brown, E.N., and Wilson, M.A. (2014). State-dependent architecture of thalamic reticular subnetworks. Cell *158*, 808–821. https://doi.org/10.1016/j.cell.2014.06.025.

Halassa, M.M., and Sherman, S.M. (2019). Thalamocortical circuit motifs: a general framework. Neuron *103*, 762–770. https://doi.org/10.1016/j.neuron.2019.06.005.

Huang, J., Polgar, E., Solinski, H.J., Mishra, S.K., Tseng, P.Y., Iwagaki, N., Boyle, K.A., Dickie, A.C., Kriegbaum, M.C., Wildner, H., et al. (2018). Circuit dissection of the role of somatostatin in itch and pain. Nat. Neurosci. *21*, 707–716. https://doi.org/10.1038/s41593-018-0119-z.

Huang, T.W., Lin, S.H., Malewicz, N.M., Zhang, Y., Zhang, Y., Goulding, M., LaMotte, R.H., and Ma, Q.F. (2019). Identifying the pathways required for coping behaviors associated with sustained pain. Nature *565*, 86–90. https://doi.org/10.1038/s41586-018-0793-8.

Jeong, K.Y., Kim, H.M., and Kang, J.H. (2016). Investigation of the functional difference between the pathological itching and neuropathic pain-induced rat brain using manganese-enhanced MRI. Acta Radiol. *57*, 861–868. https://doi.org/10.1177/0284185115604514.

Khasabov, S.G., Truong, H., Rogness, V.M., Alloway, K.D., Simone, D.A., and Giesler, G.J., Jr. (2020). Responses of neurons in the primary somatosensory cortex to itch- and pain-producing stimuli in rats. J. Neurophysiol. *123*, 1944–1954. https://doi.org/10.1152/jn.00038.2020.

Koch, S.C., Acton, D., and Goulding, M. (2018). Spinal circuits for touch, pain, and itch. Annu. Rev. Physiol. *80*, 189–217. https://doi.org/10.1146/annurev-physiol-022516-034303.

Kuner, R., and Kuner, T. (2021). Cellular circuits in the brain and their modulation in acute and chronic pain. Physiol. Rev. *101*, 213–258. https://doi.org/10.1152/physrev.00040.2019.

Lam, Y.W., and Sherman, S.M. (2007). Different topography of the reticulothalmic inputs to first- and higher-order somatosensory thalamic relays revealed using photostimulation. J. Neurophysiol. *98*, 2903–2909. https://doi.org/10.1152/jn.00782.2007.

Lee, S.M., Friedberg, M.H., and Ebner, F.F. (1994). The role of GABA-mediated inhibition in the rat ventral posterior medial thalamus. I. Assessment of receptive field changes following thalamic reticular nucleus lesions. J. Neurophysiol. *71*, 1702–1715. https://doi.org/10.1152/jn.1994.71.5.1702.

Li, Y., Lopez-Huerta, V.G., Adiconis, X., Levandowski, K., Choi, S., Simmons, S.K., Arias-Garcia, M.A., Guo, B., Yao, A.Y., Blosser, T.R., et al. (2020). Distinct subnetworks of the thalamic reticular nucleus. Nature *583*, 819–824. https://doi.org/10.1038/s41586-020-2504-5.

Lipshetz, B., Khasabov, S.G., Truong, H., Netoff, T.I., Simone, D.A., and Giesler, G.J., Jr. (2018). Responses of thalamic neurons to itch- and pain-producing stimuli in rats. J. Neurophysiol. *120*, 1119–1134. https://doi.org/10.1152/jn.00264.2018.

Luo, C., Kuner, T., and Kuner, R. (2014). Synaptic plasticity in pathological pain. Trends Neurosci. *37*, 343–355. https://doi.org/10.1016/j.tins.2014.04.002.

Ma, Q. (2010). Labeled lines meet and talk: population coding of somatic sensations. J. Clin. Invest. *120*, 3773–3778. https://doi.org/10.1172/JCI43426.

Marlinski, V., Sirota, M.G., and Beloozerova, I.N. (2012). Differential gating of thalamocortical signals by reticular nucleus of thalamus during locomotion. J. Neurosci. *32*, 15823–15836. https://doi.org/10.1523/JNEUROSCI.0782-12.2012.

Martinez-Garcia, R.I., Voelcker, B., Zaltsman, J.B., Patrick, S.L., Stevens, T.R., Connors, B.W., and

Cruikshank, S.J. (2020). Two dynamically distinct circuits drive inhibition in the sensory thalamus. Nature *583*, 813–818. https://doi.org/10.1038/s41586-020-2512-5.

Meixiong, J., and Dong, X.Z. (2017). Mas-related G protein-coupled receptors and the biology of itch sensation. Annu. Rev. Genet. *51*, 103–121. https://doi.org/10.1146/annurev-genet-120116-024723.

Mochizuki, H., Baumgartner, U., Kamping, S., Ruttorf, M., Schad, L.R., Flor, H., Kakigi, R., and Treede, R.D. (2013). Cortico-subcortical activation patterns for itch and pain imagery. Pain *154*, 1989–1998. https://doi.org/10.1016/j.pain.2013.06.007.

Mochizuki, H., and Kakigi, R. (2015). Central mechanisms of itch. Clin. Neurophysiol. *126*, 1650–1660. https://doi.org/10.1016/j.clinph.2014.11.019.

Moser, H.R., and Giesler, G.J., Jr. (2014). Characterization of pruriceptive trigeminothalamic tract neurons in rats. J. Neurophysiol. *111*, 1574–1589. https://doi.org/10.1152/jn.00668.2013.

Mu, D., Deng, J., Liu, K.F., Wu, Z.Y., Shi, Y.F., Guo, W.M., Mao, Q.Q., Liu, X.J., Li, H., and Sun, Y.G. (2017). A central neural circuit for itch sensation. Science *357*, 695–699. https://doi.org/10.1126/science.aaf4918.

Nagasaka, K., Takashima, I., Matsuda, K., and Higo, N. (2017). Late-onset hypersensitivity after a lesion in the ventral posterolateral nucleus of the thalamus: a macaque model of central post-stroke pain. Sci. Rep. *7*, 10316. https://doi.org/10.1038/s41598-017-10679-2.

Pinault, D., and Deschnes, M. (1998). Projection and innervation patterns of individual thalamic reticular axons in the thalamus of the adult rat: a three-dimensional, graphic, and morphometric analysis. J. Comp. Neurol. *391*, 180–203. https://doi.org/10.1002/(sici)1096-9861(19980209)391:2<180::Aid-cne3>3.0.Co;2-z.

Potes, C.S., Neto, F.L., and Castro-Lopes, J.M. (2006). Inhibition of pain behavior by GABA(B) receptors in the thalamic ventrobasal complex: effect on normal rats subjected to the formalin test of nociception. Brain Res. *1115*, 37–47. https://doi.org/10.1016/j.brainres.2006.07.089.

Saade, N.E., Al Amin, H., Abdel Baki, S., Safieh-Garabedian, B., Atweh, S.F., and Jabbur, S.J. (2006). Transient attenuation of neuropathic manifestations in rats following lesion or reversible block of the lateral thalamic somatosensory nuclei. Exp. Neurol. *197*, 157–166. https://doi.org/10.1016/j.expneurol.2005.09.005.

Samineni, V.K., Grajales-Reyes, J.G., Grajales-Reyes, G.E., Tycksen, E., Copits, B.A., Pedersen, C., Ankudey, E.S., Sackey, J.N., Sewell, S.B., Bruchas, M.R., et al. (2021). Cellular, circuit and transcriptional framework for modulation of itch in the central amygdala. Elife *10*. https://doi.org/10.7554/eLife.68130.

Sanders, K.M., Sakai, K., Henry, T.D., Hashimoto, T., and Akiyama, T. (2019). A subpopulation of amygdala neurons mediates the affective component of itch. J. Neurosci. *39*, 3345–3356. https://doi.org/10.1523/JNEUROSCI.2759-18.2019.

Shields, S.D., Eckert, W.A., 3rd, and Basbaum, A.I. (2003). Spared nerve injury model of neuropathic pain in the mouse: a behavioral and anatomic analysis. J. Pain *4*, 465–470. https://doi.org/10.1067/s1526-5900(03)00781-8.

Steinhoff, M., Schmelz, M., Szabó, I.L., and Oaklander, A.L. (2018). Clinical presentation, management, and pathophysiology of neuropathic itch. Lancet Neurol. *17*, 709–720. https://doi.org/10.1016/s1474-4422(18)30217-5.

Tervo, D.G., Hwang, B.Y., Viswanathan, S., Gaj, T., Lavzin, M., Ritola, K.D., Lindo, S., Michael, S., Kuleshova, E., Ojala, D., et al. (2016). A designer AAV variant permits efficient retrograde access to projection neurons. Neuron *92*, 372–382. https://doi.org/10.1016/j.neuron.2016.09.021.

Tinnermann, A., Buchel, C., and Cohen-Adad, J. (2021). Cortico-spinal imaging to study pain. Neuroimage *224*, 117439. https://doi.org/10.1016/j.neuroimage.2020.117439.

Todd, A.J. (2010). Neuronal circuitry for pain processing in the dorsal horn. Nat. Rev. Neurosci. *11*, 823–836. https://doi.org/10.1038/nrn2947.

Wang, H., Dong, P., He, C., Feng, X.Y., Huang, Y., Yang, W.W., Gao, H.J., Shen, X.F., Lin, S., Cao, S.X., et al. (2020). Incerta-thalamic circuit controls nocifensive behavior via cannabinoid type 1 receptors. Neuron *107*, 538–551.e7. https://doi.org/10.1016/j.neuron.2020.04.027.

Xu, S., Yang, H., Menon, V., Lemire, A.L., Wang, L., Henry, F.E., Turaga, S.C., and Sternson, S.M. (2020). Behavioral state coding by molecularly defined paraventricular hypothalamic cell type ensembles. Science *370*, eabb2494. https://doi.org/10.1126/science.abb2494.

Yang, C.F., Chiang, M.C., Gray, D.C., Prabhakaran, M., Alvarado, M., Juntti, S.A., Unger, E.K., Wells, J.A., and Shah, N.M. (2013). Sexually dimorphic neurons in the ventromedial hypothalamus govern mating in both sexes and aggression in males. Cell *153*, 896–909. https://doi.org/10.1016/j.cell.2013.04.017.

Zhang, C., Chen, R.X., Zhang, Y., Wang, J., Liu, F.Y., Cai, J., Liao, F.F., Xu, F.Q., Yi, M., and Wan, Y. (2017). Reduced GABAergic transmission in the ventrobasal thalamus contributes to thermal hyperalgesia in chronic inflammatory pain. Sci. Rep. *7*, 41439. https://doi.org/10.1038/srep41439.

Zhang, F.X., Ge, S.N., Dong, Y.L., Shi, J., Feng, Y.P., Li, Y., Li, Y.Q., and Li, J.L. (2018). Vesicular glutamate transporter isoforms: the essential players in the somatosensory systems. Prog. Neurobiol. *171*, 72–89. https://doi.org/10.1016/j.pneurobio.2018.09.006.

Zhu, Y.B., Xu, L., Wang, Y., Zhang, R., Wang, Y.C., Li, J.B., and Mu, D. (2020). Posterior thalamic nucleus mediates facial histaminergic itch. Neuroscience *444*, 54–63. https://doi.org/10.1016/j.neuroscience.2020.07.048.

Zhu, X., Tang, H.D., Dong, W.Y., Kang, F., Liu, A., Mao, Y., Xie, W., Zhang, X., Cao, P., Zhou, W., et al. (2021). Distinct thalamocortical circuits underlie allodynia induced by tissue injury and by depression-like states. Nat. Neurosci. *24*, 542–553. https://doi.org/10.1038/s41593-021-00811-x.

STAR★METHODS

KEY RESOURCES TABLE

REAGENT or RESOURCE	SOURCE	IDENTIFIER
Antibodies		
Guinea Pig anti-NeuN	Millipore	Cat#ABN90; RRID:AB_11205592
Donkey anti-Guinea Pig IgG-Alexa Cy3	Jackson ImmunoResearch Laboratories	Cat#706-545-148; RRID:AB_2340472
Streptavidin, Alexa Fluor 488 conjugates	Invitrogen	Cat#S11223
Bacterial and virus strains		
AAV2/8-hSyn-GCaMP6s	Shanghai Taitool	Cat#S0225
AAV2/8-CAG-DIO-GCaMP6s	Shanghai Taitool	Cat#S0354
AAV2/9-hSyn-hM4Di-mCherry	Shanghai Taitool	Cat#S0279
AAV2/8-CAG-DIO-*Gt*ACR1-P2A-EGFP	Shanghai Taitool	Cat#S0311-5-H20
AAV2/9-EF1α-DIO-eNpHR3.0-EYFP	Shanghai ObiO	Cat#AG26966
AAV2/9-EF1α-DIO-hM3Dq-mCherry	Shanghai ObiO	Cat#HYMBH3538
AAV2/2-hSyn-Cre	Shanghai Taitool	Cat#S0278-2RP-H20
AAV2/9-EF1α-DIO-ChR2-mCherry	Shanghai ObiO	Cat#AG20297
AAV2/5-CAG-DIO-taCaspase3-TEVp	Shanghai Taitool	Cat#S0236-5-H20
Chemicals, peptides, and recombinant proteins		
Picrotoxin	Sigma-Aldrich	Cat#R284556
Biocytin	Sigma-Aldrich	Cat#B4261
Clozapine-*N*-oxide, CNO	Sigma-Aldrich	Cat#C0832
Histamine	Sigma-Aldrich	Cat#H7125
Chloroquine	Sigma-Aldrich	Cat#C6628
Experimental models: Organisms/strains		
Mouse: C57BL/6J	Shanghai SLAC Laboratory	N/A
Mouse: VGlut2-ires-Cre	Jackson Laboratory	Stock No:016963; RRID:IMSR_JAX:016963
Mouse: Vgat-ires-Cre	Jackson Laboratory	Stock No:016962; RRID:IMSR_JAX:016963
Mouse: Rosa26-tdTomato	Jackson Laboratory	Stock No:007909; RRID:IMSR_JAX:007909
Software and algorithms		
GraphPad Prism 6.0	Graphad Software	http://graphpad-prism.software.informer.com/6.0/
Fiji	Fiji	http://imagej.net/software/fiji/
MATLAB 2013b, 2014b	Mathworks	http://www.mathworks.com/downloads
Videotrack	ViewPoint Behavior Technology	http://www.viewpoint.fr/zh_CN/p/software/videotrack
AniLab software	Anilab Software & Instruments	http://www.anilab.cn/soft/anilab.asp
Zeus system	Bio-Signal Technologies, USA	https://www.bio-signal.com/
NeuroExplorer 5.2	Plexon, USA	https://plexon.com/products/offlfline-sorter/
Offline Sorter 2.8	Plexon, USA	https://www.neuroexplorer.com/

RESOURCE AVAILABILITY

Lead contact

Further information and requests for resources and reagents should be directed to and will be fulfilled by the Lead Contact, Di Mu (damonmu@163.com or dimu08207@ustc.edu).

Materials availability

This study did not generate new unique reagents.

Data and code availability

All relevant datasets and analysis are included in this article and in the supplemental information, or are available from the Lead Contact upon reasonable request.

All original code is available from the Lead Contact upon reasonable request.

Any additional information required to reanalyze the data reported in this work paper is available from the Lead Contact upon request.

EXPERIMENTAL MODEL AND SUBJECT DETAILS

Male wild-type *C57BL/6J*, *VGlut2-ires-Cre, Vgat-ires-Cre, Rosa26-tdTomato* mice (postnatal 60 to 80 days) were used for experiments. *C57BL/6J* mice were purchased from SLAC Laboratory (Shanghai). *VGlut2-ires-Cre* (Stock No:016963) mice, *Vgat-ires-Cre* mice (Stock No:016962), and *Rosa26-tdTomaoto* (Stock No:007909) were initially acquired from the Jackson Laboratory and given by Dr. Yan-Gang Sun and Dr. Hua-Tai Xu. All mice were raised on a 12-hr light/dark cycle (lights on at 7:00 am) with *ad libitum* food and water. All behavioral tests were carried out during the light phase. All animal experiment procedures were approved by the Animal Care and Use Committee of the Animal Care and Use Committee of Shanghai General Hospital (2019AW008).

METHOD DETAILS

General surgical procedures and viral delivery

For all surgical procedures, mice were anesthetized with 1.5% isoflurane (Abbvie Pharmaceutical) at an oxygen flow rate of 1 L/min. A magnet (1 mm in diameter, 3 mm in length) was implanted under the skin on the dorsal surface of the right hindpaw to record scratching behaviors. Then, the mice were placed on the stereotaxic frame (RWD Life Science, 68513) with a heating pad to maintain the body temperature. The virus (100-200 nL) was delivered with a glass pipette (tip diameter 10-20 μm) at a rate of 50 nL/min using Picospritzer III (Parker), controlled by Master-8 (A.M.P.I.). After the injection, the glass pipettes were left in place for 10 minutes before the withdrawal. The animals were allowed to recover on a heating blanket. Antibiotic (Ceftriaxone sodium, 100 mg/kg) was injected (i.p.) for 3 consecutive days. Optical fibers were implanted 2-3 weeks after virus injection, and experiments were performed 3-4 weeks after virus injection. In TRN lesion experiment, the behavioral tests were performed 4 weeks after virus injection. At the end of the experiment, all animals were perfused to confirm the virus expression areas. Only animals with correct virus expression areas were included for analysis.

Surgery for injection into VB

For fiber photometry recording the activity of VB neurons, wild-type mice were injected with 200 nL AAV-hSyn-GCaMP6s virus (AAV2/8, titer: 4 x 10^{12} vector genomes/ml, Taitool) or AAV-hSyn-EGFP (AAV2/8, titer: 4.5 x 10^{12} v.g./ml, Taitool) as control into contralateral VB (according to the pruritogens injection site; antero-posterior (AP) -1.65 mm, medio-lateral (ML) 1.70 mm, dorsal-ventral (DV) -3.55 mm).

To inhibit the neuronal activity of the VB with DREADDs, wild-type mice were bilaterally injected with 200 nL AAV-hSyn-hM4Di-mCherry (AAV2/9, titer: 4 x 10^{12} v.g./ml, Taitool) or AAV-hSyn-mCherry (AAV2/8, titer: 4 x 10^{12} v.g./ml, Taitool) into the VB (AP -1.65 mm, ML ±1.70 mm, DV -3.55 mm).

To inhibit the neuronal activity of the VB with optogenetic, we injected 200 nL AAV-CAG-DIO-*Gt*ACR1-P2A-EGFP (AAV2/8, titer: 4 x 10^{12} v.g./ml, Taitool) virus or AAV-EF1α-DIO-EGFP (AAV2/8, titer: 4 x 10^{12} v.g./ml, Taitool) virus into the contralateral VB (according to the pruritogens injection site, AP -1.65 mm, ML 1.70 mm, DV -3.55 mm) of *VGlut2-ires-Cre* mice.

To inhibit the neuronal activity of the VB with optogenetic in SNI- and formalin-induced pain models, we injected 200 nL AAV-EF1α-DIO-eNpHR3.0-EYFP (AAV2/9, titer: 4 x 10^{12} v.g./ml, ObiO) virus or AAV-EF1α-DIO-EGFP (AAV2/8, titer: 4 x 10^{12} v.g./ml, Taitool) virus into the contralateral VB (according to the spared nerve injury side, AP -1.65 mm, ML 1.70 mm, DV -3.55 mm) of *VGlut2-ires-Cre* mice.

To increase the neuronal activity of the VB with DREADDs, we injected 200 nL AAV-EF1α-DIO-hM3Dq-mCherry (AAV2/9, titer: 1.09 x 10^{12} v.g./ml, ObiO) or AAV-EF1α-DIO-mCherry (AAV2/8, titer: 4 x 10^{12} v.g./ml, Taitool) into VB as control (AP -1.65 mm, ML ±1.70 mm, DV -3.55 mm) of *VGlut2-ires-Cre* mice bilaterally.

To retrogradely label neurons projecting to the VB, we injected 200 nL retroAAV-hSyn-Cre virus (AAV2/2, titer: 6 x 10^{12} v.g./ml, Taitool) into the left VB (AP -1.65 mm, ML 1.70 mm, DV -3.55 mm) of *Rosa26-tdTomato* mice.

Surgery for injection into TRN

To dissect projections from TRN neurons, we injected 200 nL AAV-EF1α-DIO-EGFP (AAV2/8, titer: 4 x 10^{12} v.g./ml, Taitool) into dorsal TRN (AP -1.34 mm, ML 2.0 mm, DV -3.2 mm) or ventral TRN (AP -1.34 mm, ML 2.2 mm, DV -3.6 mm) of *Vgat-ires-Cre* mice.

For electrophysiological experiments, we injected 200 nL AAV-EF1α-DIO-ChR2-mCherry (AAV2/9, titer: 4.27 x 10^{12} v.g./ml, OBiO) into the TRN (AP -1.34 mm, ML 2.2 mm, DV -3.6 mm) of *Vgat-ires-Cre* mice.

To record the neuronal activity of TRN neurons during scratching behaviors or pinch stimulus, we injected 200 nL AAV-CAG-DIO-GCaMP6s (AAV2/8, titer: 4 x 10^{12} v.g./ml, Taitool) into the contralateral TRN (according to the histamine injection site, AP -1.34 mm, ML 2.2 mm, DV -3.6 mm) of *Vgat-ires-Cre* mice.

For optogenetic activation of TRN-VB projections, we injected 200 nL AAV-EF1α-DIO-ChR2-mCherry (AAV2/9, titer: 4.27 x 10^{12} v.g./ml, OBiO) into the contralateral TRN (AP -1.34 mm, ML 2.2 mm, DV -3.6 mm) of *Vgat-ires-Cre* mice, and AAV-EF1α-DIO-mCherry (AAV2/8, titer: 4 x 10^{12} v.g./ml, Taitool) as control.

To ablate TRN neurons, we bilaterally injected 200 nL AAV-CAG-DIO-taCaspase3-TEVp (AAV2/5, titer: 4 x 10^{12} v.g./ml, Taitool) or AAV-EF1α-DIO-EGFP (AAV2/8, titer: 4 x 10^{12} v.g./ml, Taitool) into TRN (AP -1.34 mm, ML ± 2.2 mm, DV -3.6 mm) of *Vgat-ires-Cre* mice.

Implantation of optical fibers in the VB or TRN

The mice were implanted with optical fibers (numerical aperture, NA 0.37, 200 μm in diameter, AniLab) two weeks after virus injection. Optical fibers were attached to the skull with dental cement. For fiber photometry recording of VB neurons, the animals were implanted with optical fibers targeting 50 μm above the virus injection coordinates. For optogenetic inhibition of the VB neurons, the animals were implanted with optical fibers targeting 100 μm above the virus injection coordinates.

For fiber photometry recording of TRN neurons, the animals were implanted with optical fibers into the contralateral TRN at 15 degrees targeting 50 μm above the virus injection coordinates. For fiber photometry recording the TRN-VB projecting fibers, the animals were implanted with optical fibers into the contralateral VB (AP -1.65 mm, ML 1.70 mm, DV -3.50 mm). For optogenetic activation of TRN-VB projection fibers, the animals were implanted with optical fibers into contralateral VB (AP -1.65 mm, ML 1.70 mm, DV -3.50 mm).

At the end of the experiment, all animals were perfused to confirm the optical fiber sites. Only animals with correct optical fiber sites and virus expression regions were included for analysis.

Fiber photometry

The mice for calcium recording in soma were implanted with optical fibers 2-3 weeks after virus injection. And the mice for calcium recording in TRN-VB projection fibers were implanted with optical fibers 3-4 weeks after virus injection to get the better expression of GCaMP6s. Mice were allowed to recover for one week after optical fiber implantation and were handled 20 minutes daily for one week before fiber photometry recording. The scratching behavior and Ca^{2+} transient signal were recorded simultaneously by a custom-made recording system (Thinker-bioteck) after intradermal injection of histamine or chloroquine into the neck. The scratching behavior was recorded at 1000 Hz, and calcium transient was recorded at 50 Hz.

To evaluate the calcium activity of VB neurons or TRN-VB projections during a pinch, we used a plastic tweezer to pinch the neck skin or the tail. A Transistor-Transistor Logic (TTL) signal was manually generated

by the Master-9 Pulse Stimulator (AMPI) and synchronized with the stimulus. The TTL signal was recorded at 1000 Hz, and calcium transient was recorded at 50 Hz.

The data for fiber photometry and scratching behavior recording was analyzed using MATLAB. After subtracting the noise signal of the fiber photometry recording system, the values of Ca^{2+} transients change ($\Delta F/F$) from 3.5 s preceding scratching train onset and 5 s after scratching train onset were derived by calculating $(F\text{-}F_0)/F_0$, where F refers to the fluorescence values at each time point (-3.5 s to 5 s relative to the scratching train onset), and F_0 refers to the median of the fluorescence values during the baseline period (-2 s to -1 s relative to the scratching train onset). The onset period was defined as 1.5 s to 2 s relative to the scratching train onset, and the -0.2 s to 0.2 s was defined as onset point.

For pinch stimulus, the values of Ca^{2+} transients change ($\Delta F/F$) from 2 s preceding pinch onset and 2 s after pinch onset were derived by calculating $(F\text{-}F_0)/F_0$, where F refers to the fluorescence values at each time point (-2 s to 2 s relative to the pinch onset), and F_0 refers to the median of the fluorescence values during the baseline period (-1 s to -0.5 s relative to pinch onset). The 0.25 s to 0.5 s was defined as the onset period. To visualize the fluorescence change, the $\Delta F/F$ values of each scratching train or each pinch stimulus were heat plotted for each mouse and averaged. $\Delta F/F$ values of mice within a group were then averaged and plotted with a shaded area indicating the SEM.

Itch behavior test

We first performed the locomotion tests, then the itch-scratching tests, and nociception tests in the last. Mice were shaved on the right nape of the neck and individually handled 20 minutes daily for five consecutive days before behavioral tests. The behavior-recording system and magnetic induction method were custom-made by Shanghai Deayea Technology. The total movement (including walking and scratching) of the magnet induced a small voltage change was recorded at 1000 Hz. On the test day, the baseline was recorded for 15 minutes, and then the mice were intradermally injected with pruritic compounds into the right neck. In the optogenetic inhibition of VB activity or optogenetic activation of TRN-VB projections experiments, histamine (500 μg/50 μL; Sigma) and chloroquine (200 μg/50 μL; Sigma) were used. In the chemogenetic activation of VB activity or the ablation of the TRN experiments, histamine (300 μg/30 μL) and chloroquine (120 μg/30 μL) were used. Scratching behaviors were recorded for 30-36 minutes after injection. The data were analyzed with custom-written codes in MATLAB. The experiments were performed in a double-blind manner.

Analysis of the scratching behaviors

The walking movement signals and scratching signals were recorded with our behavior-recording system, and they exhibited different characteristics: each walking movement signal contained a single voltage peak, while scratching induced a cluster of voltage peaks. Scratching bouts were defined as a cluster of peaks (including at least three consecutive peaks) with an inter-peak interval < 0.2 s (the frequency of scratching events in a scratching bout greatly varied between 5 and 45 Hz by manual analysis of the scratching trains). A scratching train was defined as a cluster of scratching bouts with an interbout interval < 3.5 s. Other peaks above the threshold were considered as other motion (mainly waking) events. The data was first automatically analyzed and then manually adjusted by a customized graphical user interface program to detect missed scratching events and delete false scratching events.

Nociceptive behavior

Animals were habituated to the behavioral room for at least two days before behavioral tests. For testing mechanical sensitivity, the mouse hindpaw was perpendicularly stimulated with a series of von Frey hairs with logarithmically incrementing stiffness (0.16, 0.4, 0.6, 1.0, 1.4, 2.0 gram). The 50% paw withdrawal threshold was determined using the Up-Down method. For examining thermal sensitivity, the paw withdrawal latency to a noxious thermal stimulus was determined as the average of at least four measurements on the paw using the Hargreaves apparatus, with a cut-off time of 20 s to avoid tissue damage.

Spared nerve injury model

Spared nerve injury (SNI) of the sciatic nerve was performed two weeks after virus injection and optical fiber implantation (Shields et al., 2003). In brief, the mice were anesthetized with isoflurane, then the skin and muscle of the left thigh were incised to explore the sciatic nerve. After exposure, axotomy and ligation

of the tibial and common peroneal nerves were performed, leaving the sural nerve intact. Muscle and skin were closed in two layers.

Formalin test

Formalin test was performed two weeks after virus injection and optical fiber implantation. Briefly, mice were placed in a transparent enclosure for a 10 minutes habituation period. An intraplantar injection of formalin (4%, 10 μL) into the plantar of the right hindpaw and a video recording was performed. The licking or biting time was counted in a 5-minutes interval. Phase I (0-10 minutes) and phase II (10-60 minutes) pain responses were quantified.

Open field test

Locomotor activity was tested in polystyrene enclosures (40 x 40 x 40 cm). Mice were placed in the center of the box and were videotaped individually. The center area was defined as centric 20 x 20 cm. The track was analyzed by Viewpoint software and AniLab software. Total distance traveled, the velocity, and the time spent in the center area were analyzed.

Rotarod

On the first two days, mice were placed on a rotarod apparatus (Med Associates) that accelerated 5-20 revolutions per minute (r.p.m.) for 5 minutes and trained to maintain their balancing walking. On the third day, the rod accelerated 5-40 r.p.m. and mice were tested twice with a maximum time of 300 seconds. The latencies of animals falling off were assessed.

Chemogenetic manipulations

For *in vivo* chemogenetic manipulation of VB, mice were injected with clozapine N-oxide (CNO, i.p., 1 mg/kg, Sigma). Histamine, chloroquine-induced, or spontaneous scratching behavior tests or other behavioral tests were performed 30 minutes later.

Optogenetic manipulations

For *Gt*ACR1 optogenetic inhibition of VB neurons in itch experiments, scratching behaviors were recorded for 36 minutes, composed of 6 repeated 3-minutes laser OFF/3-minutes laser ON cycles. Constant 473 nm (6 mW, CrystaLaser) laser was delivered during the laser ON phase, controlled by Master-9 (A.M.P.I.). To examine the effect of optogenetic inhibition of the VB by *Gt*ACR1 on locomotion activity, mice were tested for a 15-minutes session (5-minutes laser OFF, 5-minutes laser ON, and 5-minutes laser OFF periods). A constant 473 nm laser (6 mW) was delivered during the laser ON phase. To assess the effects of *Gt*ACR1 inhibition of VB activity on the basal nociception, a constant 473 nm laser (6 mW) was delivered for 15 seconds during each trail.

To assess the effects of eNpHR3.0 inhibition of VB activity on the SNI model, a constant 593 nm laser (4 mW, CrystaLaser) was delivered for 15 seconds in each trial. To assess the effects of eNpHR3.0 inhibition of VB activity on the formalin model, a constant 593 nm laser (4 mW) was delivered for 60 minutes.

For ChR2 activation of TRN-VB projections in itch experiments, the scratching behaviors were recorded for 36 minutes, composed of 6 repeated 3-minute laser OFF/3-minute laser ON cycles. The 473 nm laser (2 ms, 4 mW, 20 Hz) was delivered during laser ON phases. To examine the effect of optogenetic activation of TRN-VB projections on locomotion activity, mice were tested for a 15-minute session (5-minute laser OFF, 5-minute laser ON, and 5-minute laser OFF periods). The 473 nm laser (2 ms, 4 mW, 20 Hz) was delivered during the laser ON phase. To assess the effect of ChR2 activation of TRN-VB projections on the basal nociception, the 473 nm laser (2 ms, 4 mW, 20 Hz) was delivered for 15 seconds during each trial. To determine the effect of ChR2 activation of TRN-VB projections on the SNI model, 473 nm laser (2 ms, 4 mW, 20 Hz) was delivered for 15 seconds in each trial. To determine the effect of ChR2 activation of TRN-VB projections on the formalin model, 473 nm laser (2 ms, 4 mW, 20 Hz) was delivered for 60 minutes.

Brain slice electrophysiology

Mice were anesthetized with isoflurane and perfused transcardially with an ice-cold cutting solution containing (in mM): sucrose 213, KCl 2.5, NaH_2PO_4 1.25, $MgSO_4$ 10, $CaCl_2$ 0.5, $NaHCO_3$ 26, glucose 11 (300-305 mOsm). The brain was rapidly dissected, and coronal slices (280 μm) were sectioned, using a

vibratome (VT1200S, Leica) at a slicing speed of 0.12 mm/s and a blade vibration amplitude of 0.8 mm. Slices were transferred into holding chamber and incubated in 34°C artificial cerebrospinal fluid (ACSF) containing (in mM): NaCl 126, KCl 2.5, NaH_2PO_4 1.25, $MgCl_2$ 2, $CaCl_2$ 2, $NaHCO_3$ 26, glucose 10 (300-305 mOsm). After 30 minutes of recovery, slices were kept at room temperature. Both cutting solution and ACSF were continuously bubbled with 95% O_2/5% CO_2. Then, slices were placed on glass coverslips coated with poly-L-lysine (Sigma) and submerged in a recording chamber. All experiments were performed at near-physiological temperatures (30-32°C) using an in-line heater (Warner Instruments) while perfusing the recording chamber with ACSF at 3 mL/min using a pump (HL-1, Shanghai Huxi). Whole-cell patch-clamp recordings were made from the target neurons under IR-DIC visualization and a CCD camera (Retiga ELECTRO, QIMAGING) using a fluorescent Olympus BX51WI microscope. Recording pipettes (2−5 MΩ; Borosilicate Glass BF 150-86-10; Sutter Instrument) were prepared by a micropipette puller (P97; Sutter Instrument) and backfilled with potassium-based internal solution containing (in mM) K-gluconate 130, $MgCl_2$ 1, $CaCl_2$ 1, KCl 1, HEPES 10, EGTA 11, Mg-ATP 2, Na-GTP 0.3 (pH 7.3, 290 mOsm) or cesium-based internal solution contained (in mM) $CsMeSO_3$ 130, $MgCl_2$ 1, $CaCl_2$ 1, HEPES 10, QX-314 2, EGTA 11, Mg-ATP 2, Na-GTP 0.3 (pH 7.3, 295 mOsm). Biocytin (0.2%) was included in the internal solution.

In DREADDs experiments, virus infected neurons in VB were recorded in a current-clamp with 0 pA (I = 0 mode) with pipettes filled with a potassium-based internal solution. After we recorded spontaneous firing for 3 minutes, 5 μM CNO was washed in by bath for 5 minutes. Firing rates calculation was performed in 2 different periods (60 seconds for each period). The baseline firing rate was calculated 1 minute before the application of CNO. The CNO effect was calculated between 4 to 5 minutes since CNO was washed in. In VB *Gt*ACR1 experiments, *Gt*ACR1 $^{+}$ neurons or control GFP^{+} in the VB were recorded in whole-cell current-clamp configuration, and 50 pA current was injected to induce stable firing. The 473 nm laser (CL473-050, 8 mW/mm^2) coupled to a water objective (60x, NA 1.0) was used to activate *Gt*ACR1.

In TRN ChR2 experiments, whole-cell recordings with current-clamp with 0 pA (I = 0 pA mode) were obtained with pipettes filled with a potassium-based internal solution. The 473 nm laser (1 ms, 4 mW/mm^2) was used to activate ChR2. Picrotoxin (100 μM) was used to block the IPSCs evoked by the laser.

All chemicals were obtained from Sigma.

Immunohistochemical staining

Mice were anesthetized with Zoletil 50 (75 mg/kg, i.p.) and perfused with normal saline and ice-cold phosphate-buffered saline (PBS) containing 4% paraformaldehyde (PFA). Brains were carefully removed and postfixed in 4% PFA for 6-8 hours, followed by cryoprotection in 30% sucrose in PBS at 4°C. Free-floating brain sections were sectioned at 40 μm thickness with the Cryostat (Leica CM 1950). The sections were blocked for 30 minutes at room temperature in 5% normal donkey serum in PBST (0.3% Triton X-100 in PBS), followed by incubation with primary antibodies in PBST (with 1% normal donkey serum) at 4°C overnight and secondary antibodies in PBS at room temperature for 2 hours. The primary antibody used in immunohistochemistry experiments was Guinea Pig anti-NeuN (1:2000, Millipore, ABN90). The secondary antibody used in our study were donkey anti-Guinea Pig IgG-Alexa Cy3 (1:400, Jackson ImmunoResearch Laboratories, 706-545-148) and streptavidin Alexa 488 (1:400, Invitrogen, S11223). Photomicrographs of the brain sections were taken under a Nikon E600FN Neurolucida microscope (10x) and a laser-scanning confocal microscope (SP8, Leica). Images were analyzed manually using Fiji.

Extracellular recording

A 16-channel electrode was slowly inserted into the contralateral VB (according to the pruritogens injection site), and the ground wire was connected to the cranial nail. The gel (Vetbond Adhesive, 3M) and dental cement were applied to the skull surface to fix the electrode.

The mice were handled gently and acclimated to the recording environment for two days. The behavior recording system and magnetic induction recording principle were the same as reported in the literature (Mu et al., 2017). On the test day, the mice were acclimated to the recording environment for at least 30 minutes. Histamine or chloroquine was injected intradermally on the right nape of the neck of the mice to induce scratching behaviors. Itch behavior and neuronal firing in VB regions were recorded simultaneously for 30 minutes after the injection of pruritic agents. Zeus system (Bio-Signal Technologies: McKinney, TX, U.S.A) was used to collect peak potentials with a sampling frequency of 3 kHz. At the end of the experiment,

the recording sites were identified. Only the animals with the correct electrode tip sites were included for analysis.

For recording in nociceptive mechanical stimulation, von Frey filament (2 g) was applied to stimulate the right nape of the neck, and the neuronal firing was recorded simultaneously. Each filament is stimulated ten times with an interval of more than one minute. The time interval between each above-mentioned stimulus (including itch agent injection and mechanical stimulation) was at least 24 hours with the aim to minimize sensory sensitization.

Preprocessing of raw data was performed using Offline Sorter V2.8 (Plexon, USA). The raw signals were low-cut filtered (250 Hz) before waveform detection. Clusters associated with individual neurons were isolated automatically by K-mean and valley-seeking algorithms following principal components analysis. The inter-spike intervals (ISIs) less than 1 ms (refractory period) were removed before further analysis. All well-isolated neurons were further analyzed using Neuroexplorer V5.2 (Plexon, USA) and customized codes written in MATLAB 2014a (MathWorks). The peri-event time histograms (PETHs) were calculated with individual scratching onset as reference (Gao et al., 2019). The initial firing rate values were averaged with 30 ms bins and smoothed by a Gaussian window of 210 ms. The smoothed values (from -2 s to 2 s) were *z*-score normalized against mean and standard deviation (SD) of a basal epoch defined between -2 s and -1 s. Neuronal activity patterns of individual units were characterized based on Wilcoxon matched-pairs signed-rank tests comparing normalized firing rate -2 s to 0 s preceding scratching or mechanical stimulus onset (FR_{pre}) to 0 s to 2 s post scratching or mechanical stimulus onset (FR_{post}). The neurons with significant change ($P<0.05$) were classified into 'Increase' ($FR_{pre} < FR_{post}$) or 'Decrease' ($FR_{pre} > FR_{post}$). While those without significant change were 'No response'. To examine the possible specificity of neural response to itch and/or pain, we compared the activity patterns of the same neuron following onsets of scratching behavior and nociceptive mechanical stimulus, in which itch-activated/inhibited neurons were referred to that increased/decreased during histamine and chloroquine models. Only the neurons that significantly responded to either histamine or mechanical nociceptive stimulus were defined as itch- or pain-related ones.

QUANTIFICATION AND STATISTICAL ANALYSIS

All experiments were conducted in a double-blind manner. Data were presented as mean ± SEM unless stated. The statistical analyses were performed using Prism 6 (GraphPad Software) and MATLAB 2013b (MathWorks). Paired two-sided t-test and one-way ANOVA were used in fiber photometry. Wilcoxon matched-pairs signed-rank test was used in *in vivo* extracellular recordings. Paired two-sided t-test and unpaired two-sided t-test were used in the brain slice recordings. Unpaired two-sided t-test, one-way ANOVA, two-way ANOVA, and two-way repeat ANOVA analysis with Bonferroni *post hoc* test were used in behavioral tests. The cut-off for significance was held at $p = 0.05$.